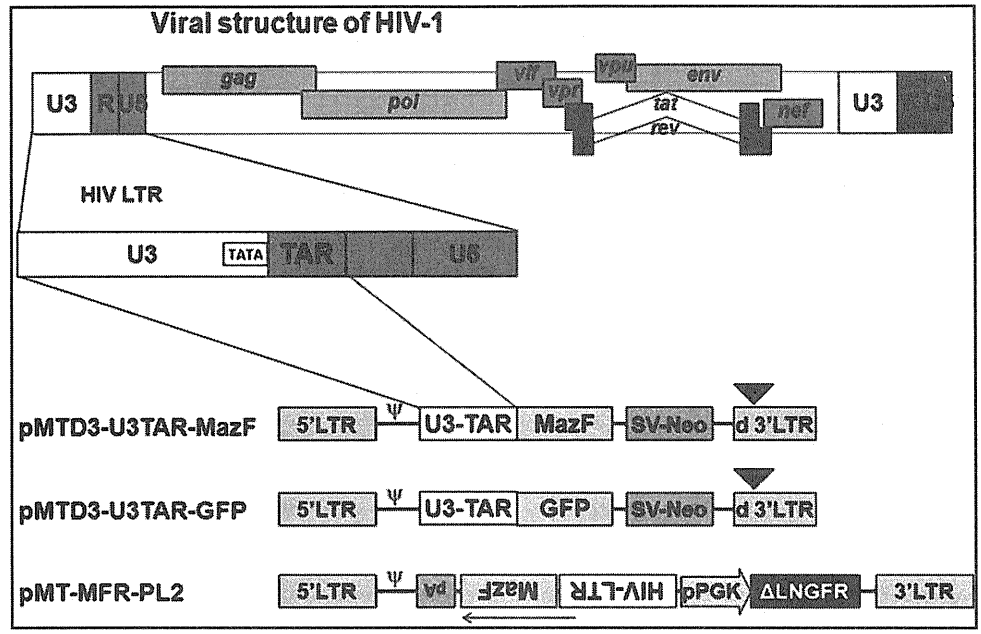


FIG. 1. Construction of retroviral vector under the control of HIV-LTR promoter. To remove promoter activity of the MoMLV LTR, the self-inactivating retroviral vector pMTD3 was constructed based on pMT (Lee *et al.*, 2004) by deleting a 276-bp fragment from its 3'LTR U3 region. A synthetic ACA-less *mazF* gene was then inserted downstream of HIV-1 U3-TAR resulting in the self-inactivating retroviral vector, pMTD3-U3TAR-MazF. As a control, the GFP gene was inserted in place of the *mazF* gene, which resulted in pMTD3-U3TAR-GFP. The self-inactivating retroviral vectors were generated using the transient transfection method with the packaging plasmids MoMLV-gag-pol, GALV-env, and the self-inactivating retroviral vector in 293T cells. The viral preparation was obtained 2 days after transfection by filtering the culture supernatant. To improve the viral titer for efficient gene transduction over an initial vector, HIV-LTR-MazF-polyA cassette was inserted in the opposite direction of the MoMLV-LTR at the multi-cloning site of pMT. A truncated form of the human low-affinity nerve growth factor gene (ΔLNGFR) (Verzeletti *et al.*, 1998) was used as a surface marker. The resultant vector plasmid was designated pMT-MFR-PL2. GALV-env retroviral vector was generated as described in Materials and Methods.

### *Retroviral transduction into primary rhesus macaque CD4+ T cells*

Rhesus macaque CD4+ T cells were isolated from peripheral blood mononuclear cells (PBMC) using anti-CD4 monoclonal antibody-conjugated beads (Dynal CD4 Positive Isolation Kit; Invitrogen). Prior to gene transduction, the isolated CD4+ T cells were activated for 3 days with a combination of anti-monkey-CD3 clone FN-18 (BioSource, Camarillo, CA) and anti-human-CD28 monoclonal antibody clone L293 (BD Biosciences, Franklin Lakes, NJ)-conjugated beads at a cell-to-bead ratio of 1:1 in GT-T503 (Takara Bio) supplemented with 10% FBS and 200 IU of interleukin-2 (Chiron, Emeryville, CA). On day 3, activated CD4+ T cells were infected with the MazF retroviral vector (MT-MFR-PL2) in the presence of RetroNectin (Takara Bio) as per the manufacturer's instructions. The transduction was repeated again on day 4. The cells were further incubated for another 3 days. The genetically modified cells marked with the ΔLNGFR+ were concentrated with anti-CD271 monoclonal antibody-conjugated beads (CD271 MicroBeads; Miltenyi Biotec, Bergisch Gladbach, Germany). Aliquots of the *mazF* gene-modified cells (designated as MazF-Tmac cells) were collected and cryopreserved until use. As a control, the nontransduced CD4+ T cells were also prepared using the same method as used above.

### *HIV infection*

CEM-SS cells and CEM-SS cells transduced with MTD3-U3TAR-MazF or MTD3-U3TAR-GFP were infected with HIV-1 IIIB at the different multiplicities of infection (MOIs) of 0.07, 0.0007, and 0.00007. After infection, cells were washed with PBS and subsequently cultured in 10 ml of RPMI 1640 containing 10% FBS. HIV-1 p24 levels in the culture supernatant were calculated using the p24 ELISA kit (PerkinElmer, Waltham, MA). Viable cell numbers were measured using the trypan blue exclusion assay. The doubling time of cells was calculated by logistic regression analysis of each growth curve for the HIV-1 infection sets.

### *SHIV infection*

The cryopreserved cells of the control CD4+ T and MazF-Tmac cells were recovered in GT-T503 medium supplemented with 10% FBS and 200 IU of interleukin-2 and reactivated with anti-monkey-CD3 and anti-human-CD28 monoclonal antibody-conjugated beads at a cell-to-bead ratio of 5:1. After a 6-day incubation, the cells were infected with simian/human immunodeficiency virus (SHIV) 89.6P (Reimann *et al.*, 1996) at the MOI of 0.01 and cultured for 6 more days. SHIV RNA levels in the culture supernatant and intracellular RNAs were determined by using quantitative real-time PCR (Thermal Cycler Dice Real Time System; Takara Bio Inc.) with a set of specific primers designed in the SHIV *gag* region (Miyake *et al.*, 2006).

### *Flow cytometry*

Flow cytometry was used for the analysis of surface CD4 expression and transduction efficiency. Endogenous expression levels of CD4 in CEM-SS cells and CEM-SS cells transduced with MTD3-U3TAR-MazF were analyzed using phycoerythrin (PE)-labeled anti-human CD4 antibody (Beckman Coulter, Fullerton, CA). Intracellular p24 levels were analyzed using fluorescein isothiocyanate-labeled anti-p24 antibody (Beckman Coulter) after the cells were fixed and permeabilized for flow cytometric analysis.

Gene transfer efficiencies of the retroviral Tat expression vector into CEM-SS cells and CEM-SS cells transduced with MTD3-U3TAR-MazF were analyzed by detecting the ZsGreen marker fluorescence. Immediately before flow cytometry, propidium iodide (PI) was added at the concentration of 100 ng/ml to stain dead cells. Samples were run through a FACSCantoII flow cytometer (BD Biosciences), and data were analyzed using the FACSDiva software (BD Biosciences).

### *Genomic DNA analysis*

Genomic DNA was extracted by phenol/chloroform extraction from CEM-SS cells and CEM-SS cells transduced with MTD3-U3TAR-MazF cells infected with HIV-1 IIIB at the MOI of 0.007. Two different regions of the HIV-1 *gag* gene (246–467 and 905–1046) were amplified by PCR at 14 days after HIV-1 IIIB infection. As a positive control, genomic DNA was amplified from H9 cells chronically infected with HIV-1 IIIB. Human mitochondrial DNA (mtDNA) was amplified as a control for the PCR.

### *Co-culture with chronically infected cells*

The CEM-SS cell line chronically infected with HIV-1 IIIB (CH-1) was mixed with CEM-SS cells or CEM-SS cells transduced with MTD3-U3TAR-MazF. CH-1 cells were mixed at different ratios of 10, 1, or 0.1%. After 6 and 14 days of infection, intracellular p24 levels were analyzed by flow cytometric analyses.

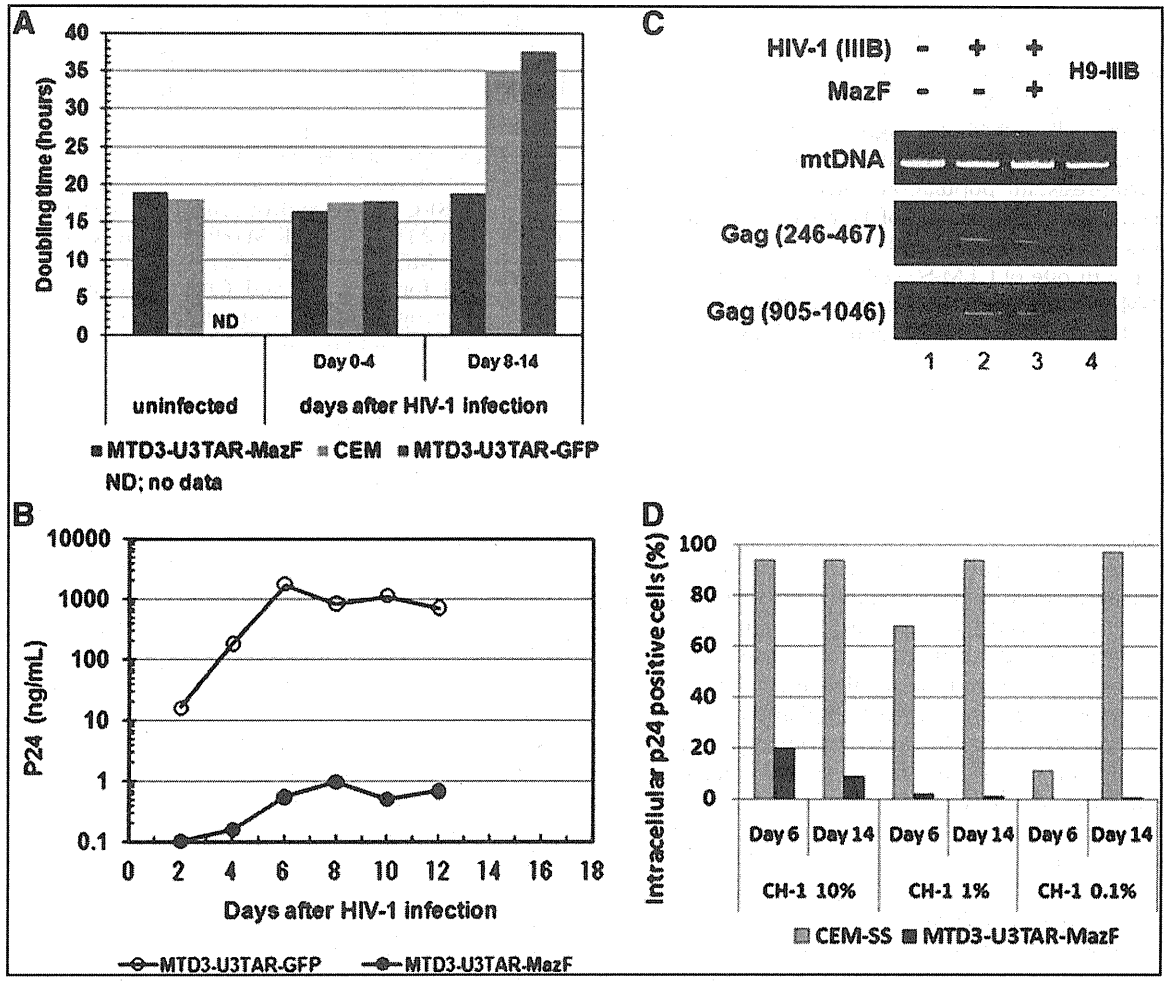


**FIG. 2.** Analysis of MazF-transduced CEM-SS cells after HIV-1 infection. (**A**) CEM-SS cells transduced with either the *mazF* gene or the GFP gene were infected with HIV-1 IIIB at an MOI of 0.07. After infection, the doubling time of the cells for each culture condition was calculated using linear regression analysis using Microsoft Excel software. The square of the correlation coefficient ($R^2$) between culture day and log (cell number) values was observed to be >0.97. (**B**) HIV-1 p24 levels in the culture supernatant were estimated using the p24 ELISA kit. Filled circles indicate p24 levels in the supernatant of CEM-SS cells transduced with MTD3-U3TAR-MazF. Open circles indicate p24 levels in the supernatant of CEM-SS cells transduced with MTD3-U3TAR-GFP. (**C**) Genomic DNA PCR analysis of CEM-SS cells and MazF-transduced CEM-SS cells infected with HIV-1 IIIB at an MOI of 0.007. Two different regions of the HIV-1 *gag* gene (246–467 and 905–1046) were amplified by PCR at 14 days after HIV-1 IIIB infection. As a positive control, the genomic DNA was amplified from H9 cells chronically infected with HIV-1 IIIB. Human mtDNA was amplified as a control for the PCR reaction. (**D**) Intracellular p24 levels were analyzed in the mixtures of CEM-SS cell lines chronically infected with HIV-1 IIIB (CH-1) using CEM-SS cells or MazF-transduced CEM-SS cells. CH-1 cells were mixed at different ratios of 10, 1, or 0.1%. After 6 and 14 days of infection, cells were stained with an anti-HIV-1 p24 antibody and subjected to flow cytometric analysis.

## Results

We first constructed the retroviral vector system in which the gene for MazF was inserted downstream of the HIV-1 TAR sequence (Fig. 1). As the *E. coli mazF* gene contains nine ACA sequences in its open-reading frame, all of these ACA sequences were first engineered to other MazF-uncleavable sequences without altering the amino acid sequence of MazF to make the *mazF* mRNA resistant to MazF. The resulting self-inactivating retroviral vector (MTD3-U3TAR-MazF) was used to transduce CD4+ T lymphoid CEM-SS cells to create a system in which MazF induction in CEM-SS cells upon infection with HIV-1 effectively suppressed HIV-1 replication without causing apoptosis of infected T cells. The MTD3 retroviral vector contained an intact 5′ LTR and a mutated 3′ LTR that lacks most of the transcriptional elements present in U3. Cells transduced with the resulting retroviral vector contained the defective LTR at both ends (Yu *et al.*, 1986). The self-inactivating retroviral vector was transiently produced and subsequently transduced into the human T lymphoid line CEM-SS cells, which are highly susceptible to HIV infection. Transduced cells were subjected to G418 selection to obtain drug-resistant populations. A GFP-expressing retroviral vector under the control of HIV-LTR (MTD3-U3TAR-GFP) was also used as a control.

The growth rate of CEM-SS cells transduced with MTD3-U3TAR-MazF was comparable to that of the parental CEM-SS line (Fig. 2A), suggesting that MazF expression was tightly controlled and did not inhibit cell growth. Furthermore, the CD4 levels of MTD3-U3TAR-MazF-transduced CEM-SS cells were identical to those of the parental CEM-SS cells (Fig. 3A).

To investigate the effects of HIV-1 infection, MazF-transduced or GFP-transduced CEM-SS cells were infected with HIV-1 IIIB at different MOIs, specifically 0.07, 0.0007, and 0.00007 (Fig. 4). Levels of the HIV-1 p24 antigen in the culture media were examined 16 days post infection. As shown in Fig. 4, in MazF-transduced CEM-SS cells, HIV-1 replication was effectively suppressed. To more precisely investigate the antiviral effects of MazF, viral production and cell growth were measured every other day after HIV-1 IIIB infection at the MOI of 0.07. As shown in Fig. 2A, in the beginning of the culture from day 0 to day 4, cell growth was similar among CEM-SS cells, MazF-transduced CEM-SS cells, and GFP-transduced CEM-SS cells, as well as uninfected CEM-SS cells. CEM-SS cells harboring the *mazF* (ACA-less) gene grew at a normal rate throughout the time course of HIV-1 IIIB infection, whereas both GFP-transduced CEM-SS cells and the parental cell line showed aberrant growth rates due to HIV-1 infection in late cultures after day 8 (Fig. 2A). Indeed, a high level of p24 was detected in the GFP-transduced cell populations during the course of infection (Fig. 2B). In the case of MazF-transduced cells, however, levels of p24 were three orders of magnitude lower than those of GFP-transduced cells throughout the experiment (Fig. 2B). Notably, CD4 levels of MazF-transduced cells infected with HIV-1 IIIB were largely unaffected (Fig. 3B). Together with the fact that the HIV-1 IIIB infected cells harboring the *mazF* gene grew normally (Fig. 2A), these results suggest that HIV-1 IIIB gene expression in the HIV-1-LTR-regulated *mazF* (ACA-less)-transduced cells is effectively inhibited by blocking HIV-1 replication with little damage to cellular function.

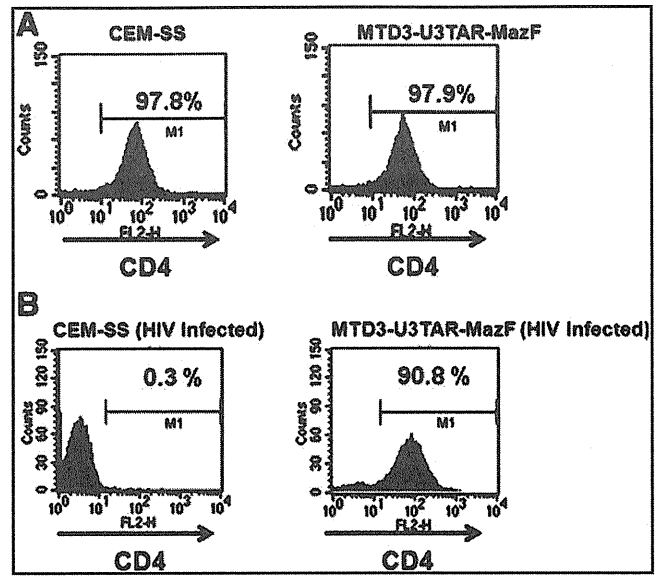


**FIG. 3.** CD4 levels in MazF-transduced cells. (**A**) Endogenous expression levels of CD4 were analyzed using PE-labeled anti-human CD4 antibody following flow cytometric analysis. (**B**) CEM-SS control cells and CEM-SS cells transduced with MTD3-U3TAR-MazF were infected with HIV-1 IIIB at an MOI of 0.007. After infection, the cells were maintained for 5 weeks and CD4 expression levels were analyzed using PE-labeled anti-human CD4 antibody following flow cytometric analysis.

Next, we examined if HIV-1 IIIB was integrated into the genome of MazF-transduced CEM-SS cells upon HIV-1 infection. Two different regions of the HIV-1 *gag* gene were amplified by PCR using genomic DNA 14 days after HIV-1 IIIB infection. As shown in Fig. 2C, both regions of the *gag* gene were detected in the genome of MazF-transduced CEM-SS cells, which were resistant to HIV-1 replication (lane 3). Similarly, HIV-1 DNA was detected in the genomes of CEM-SS cells (lane 2) and H9-IIIB cells (lane 4) (positive control H9 cells chronically infected with HIV-1 IIIB), whereas no bands were detected in noninfected cells (lane 1). We also established a CEM-SS cell line chronically infected with HIV-1 IIIB (CH-1). When this cell line was mixed with CEM-SS cells or MazF-transduced CEM-SS cells at a ratio of 10, 1, or 0.1%, CEM-SS cells were gradually infected with HIV-1 produced from CH-1 cells (Fig. 2D) and their cell growth was suppressed. Alternatively, MazF-transduced CEM-SS cells showed no growth inhibition (data not shown), indicating that HIV-1 replication was suppressed in MazF-transduced CEM-SS cells. As a result, the culture was eventually taken over by normally growing MazF-transduced CEM-SS cells over the slow-growing CH-1 cells. These data demonstrate that MazF-transduced cells are resistant to HIV-1 IIIB infection by blocking HIV-1 IIIB replication.

To investigate the *mazF* gene expression and subsequent effects more precisely, CEM-SS cells and CEM-SS cells transduced with MTD3-U3TAR-MazF were infected with the Tat-expressing retroviral vectors, M-LTR-Tat-ZG or H-LTR-Tat-ZG (Fig. 5A). Induction of the m*azF* gene in CEM-SS cells transduced with MTD3-U3TAR-MazF was monitored by real-time PCR, and the relative ratios were compared with mock infection (Fig. 5B). Infected cells were also subjected to

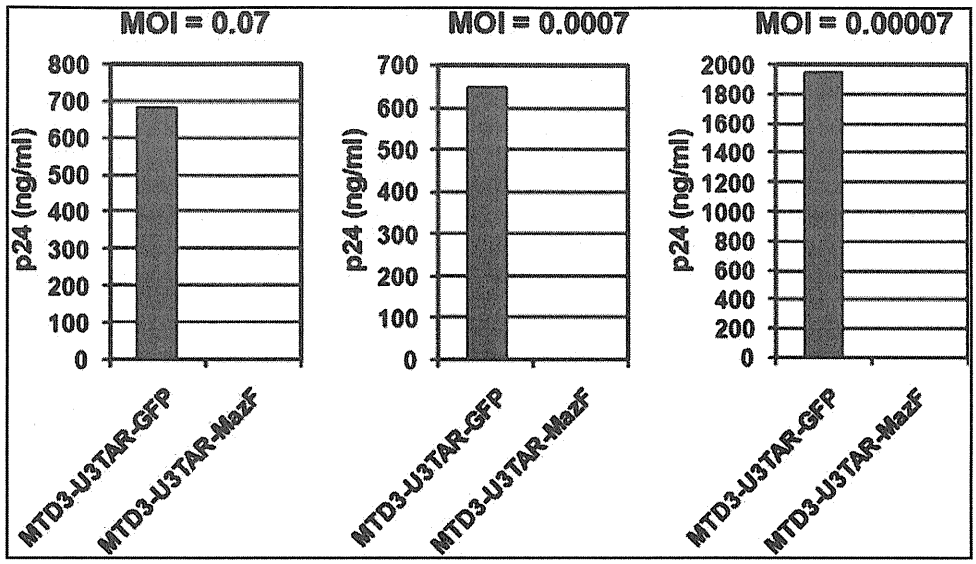


FIG. 4. HIV-1 IIIB infection using MazF-transduced CEM-SS cells at different MOIs. Polyclonal cell populations of CEM-SS resulting from gene transduction with retroviral vectors MTD3-U3TAR-MazF or MTD3-U3TAR-GFP were infected with HIV-1 IIIB at different MOIs (0.07, 0.0007, and 0.00007). Sixteen days after infection, HIV-1 p24 levels in the culture supernatant were estimated using the p24 ELISA kit (PerkinElmer). Given the cytopathic effect of HIV-1, the MTD3-U3TAR-GFP cell population showed delayed proliferation after HIV-1 infection in contrast to the MTD3-U3TAR-MazF population. The delay was more pronounced for the high-MOI group (0.07) than for the low-MOI group (0.00007) at later time points. On day 16 post infection, the accumulated cell number of the high-MOI group was threefold lower than that of the low-MOI group, so the difference in HIV-1 p24 levels between the two MOI groups (0.07 and 0.00007) reflects total cell numbers.

flow cytometry, and both Tat-positive (ZsGreen-positive) cells and dead cells (PI-positive) were monitored (Fig. 5B). As shown in Fig. 5B, strong induction of *mazF* expression was observed upon constitutive M-LTR-Tat-ZG vector transduction, and there was a significant decline in Tat-positive (ZsGreen-positive) cell population. On the other hand, *mazF* induction in HIV-LTR-driven Tat expression was lower, and the influence on cell death was also less than by MLV-LTR-driven Tat expression as observed in the PI-positive population. Although these experiments do not directly reflect HIV-1 replication, these data support the hypothesis that only low levels of MazF are expressed upon HIV-1 infection and MazF-positive cells can survive with HIV-1 provirus.

As the SIN-based retroviral vector contains the *mazF* gene in the normal orientation, the *mazF* gene is expressed from viral mRNA, resulting in the degradation of the viral RNA and thus significantly reducing the viral titer from this vector. On the other hand, when the MazF expression cassette is

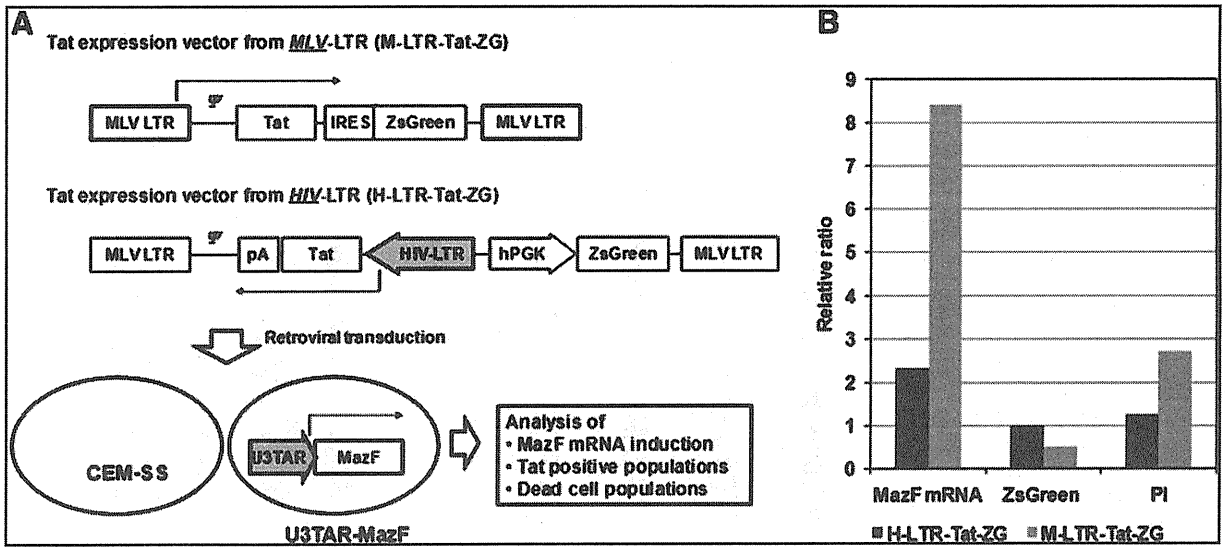


FIG. 5. Analysis of MazF induction upon Tat expression. (A) Outline of experimental procedure to analyze MazF induction upon Tat expression. (B) MazF mRNA levels were analyzed in MTD3-U3TAR-MazF transduced CEM-SS cells after Tat-expressing retroviral vector infection using real-time RT-PCR. The relative fold change is shown compared with that of mock infections. Tat-positive (ZsGreen-positive) cell populations and dead (PI-positive) cell populations in MTD3-U3TAR-MazF-transduced CEM-SS cells were analyzed by flow cytometry 2 days after different Tat retroviral vector transduction. The relative ratio is shown compared with that of CEM-SS cells.

inserted in the opposite direction from the retroviral genome, the viral titer increased and the gene transfer efficiency was improved more than 10 times (data not shown). To investigate the antiviral effect of the TAR-*mazF* system in the primary CD4+ T lymphocytes, the reversely orienting MT-MFR-PL2 vector was introduced into rhesus macaque primary CD4+ T cells from two individual monkeys (#14 and #15). The resulting *mazF*-containing cells were then infected with SIV/HIV-1 chimeric virus SHIV 89.6P. As the SHIV 89.6P harbors HIV-1-derived *env, rev, vpu,* and *tat* genes, the TAR-*mazF* system is expected to function when MazF-Tmac cells are infected with SHIV 89.6P. Indeed, efficient suppression of SHIV 89.6P replication was observed for both primary cell lines, #14 and #15 (Fig. 6A).

To evaluate further how well the retroviral *mazF* system is able to suppress viral RNA production, total cellular RNAs were extracted from MazF-Tmac cells to estimate quantitatively the amounts of SHIV RNA, as well as the mRNAs for ribosomal protein L13a (RPL13a, XM_001093017) and $\beta$-actin (NM_001033084), by real-time PCR. The relative ratios were normalized by using 18S rRNA (FJ436026), which is protected from MazF cleavage in ribosomes (Shimazu *et al.*, 2007). We obtained similar results in MazF-Tmac cells from both #14 and #15 primary cell lines. Representative results from MazF-Tmac cells from #14 are shown in Fig. 6B, where one can see that SHIV RNA was preferentially cleaved, whereas the cellular mRNAs were not affected. These results clearly demonstrate that MazF induction from the Tat system upon SHIV 89.6P infection leads to severe defect in maintaining SHIV 89.6P RNA but does not affect cellular mRNAs in SHIV-infected CD4+ T cells.

## Discussion

This study demonstrates the distinct feasibility of RNase-based strategies for gene therapy. RNase-based strategies may be preferred over RNA-based strategies for HIV therapy, because RNases cleave HIV-RNA to cause permanent damage to HIV RNA function. Additionally, as RNases function as an enzymatic catalyst, they are required only at low concentrations in the cells to effectively block HIV proliferation. In the present study, the gene for MazF, an ACA-specific mRNA interferase, was engineered under the HIV-1 LTR promoter and inserted in the genome of the CD4+ T lymphoid cells so that MazF is expected to be produced only when the cells are infected with HIV-1 to produce the Tat protein. We demonstrated that *mazF*-Tmac cells indeed acquired resistance against SHIV replication, but cell growth was not inhibited after SHIV infection (data not shown), indicating that cellular mRNAs were not significantly affected. Notably, MazF was also able to function against the expression of SHIV proviral genome, because the production of SHIV in the culture supernatant was dramatically reduced.

Acquisition of HIV-1 resistance, and more remarkably the ability of MazF-transduced cells to suppress HIV-1 replication, may be explained as follows: Upon HIV-1 infection, Tat expression is first induced from the HIV-1 proviral genome. Tat then triggers the transcription of the *mazF* gene under the LTR promoter, as well as the full-length HIV proviral genome. The resulting induction of MazF expression leads to the cleavage of newly emerged HIV-1 mRNAs so that Tat protein synthesis is no longer sustainable. However, it is important to note that HIV-1 infection does not hamper cell growth and that the HIV-1 provirus genome is retained in the MazF-transduced cells. Therefore, the cellular level of Tat appears to be maintained at a very low level so that the level of MazF induction is also kept very low enough to cleave HIV-1 mRNAs, but not cellular mRNAs. Depending on the integration site and proviral copy number, there might be some MazF-transduced cells that were not resistant to HIV-1 replication. However, these cells could not survive due to HIV-1-induced cell death.

In mammals, virus infection is known to activate the interferon response to induce RNaseL, which mediates degradation of 28S and 18S ribosomal RNAs. This results in inhibition of protein synthesis as part of the host antiviral response (Silverman, 2003). An amphibian ribonuclease,

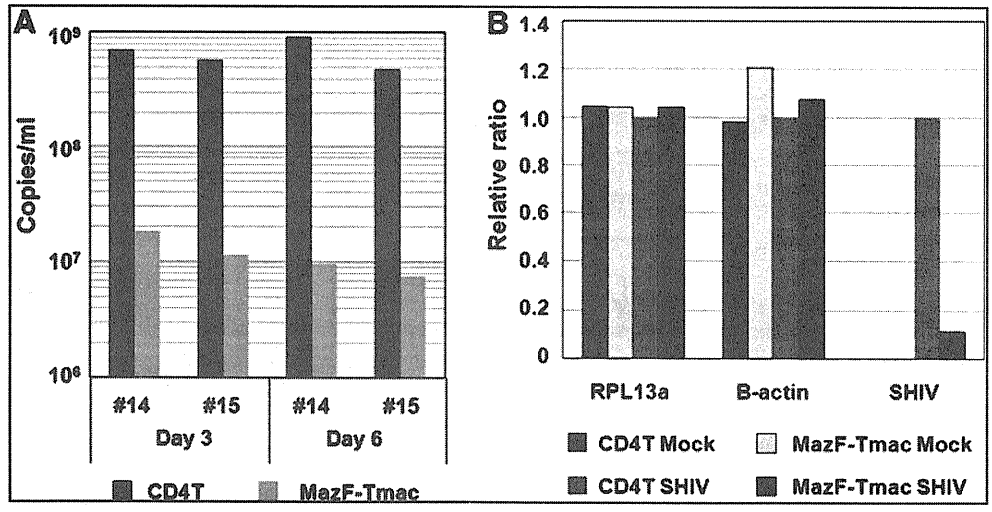


**FIG. 6.** Effect of MazF-induction into rhesus macaque primary CD4+ T cells on SHIV 89.6P replication. (**A**) Rhesus macaque primary CD4 T cells from two monkeys (#14 and #15) were activated and transduced with MT-MFR-PL2 vector. The MazF-transduced cells (MazF-Tmac cells) were reactivated with CD3/28 beads followed by infection with SHIV 89.6P. On days 3 and 6 post infection, culture supernatants were collected and evaluated for SHIV RNA copy by using the quantitative real-time PCR method. (**B**) Total cellular RNAs extracted from MazF-Tmac cells at 6 days post SHIV 89.6P infection were used to measure the amounts of SHIV RNA, as well as cellular housekeeping mRNAs, by using the quantitative real-time PCR method.

Onconase, is able to inhibit protein synthesis in mammalian cells and has been used as a protein drug. When it was added to the culture media of H9 cells persistently infected with HIV-1, HIV-1 replication was inhibited without blocking cell growth, as degradations of 18S and 28S rRNAs and cellular mRNAs were prevented (Saxena *et al.*, 1996). MazF induction in mammalian cells has shown to cause apoptotic cell death as a result of degradation of cellular mRNAs (Shimazu *et al.*, 2007). However, in the present study, MazF expression induced by HIV-1 Tat appears to be maintained at very low levels, just enough to cleave HIV-1 RNA but not cellular mRNAs, so that cells were able to grow normally. MazF expression may be autoregulated in the cell in such a way that when Tat-induced MazF eliminates invading HIV-1 RNA, Tat expression from the HIV-1 provirus is simultaneously stopped, resulting in simultaneous arrest of MazF production to recover normal cellular functions.

Targeting HIV RNA as a therapeutic strategy using antisense RNA (Levine *et al.*, 2006), ribonucleases (Agarwal *et al.*, 2006), and RNA interference (RNAi) technology (Morris and Rossi, 2004) has been attempted. However, the use of antisense RNA and RNAi technology has not been effective as an anti-HIV technology, as HIV can easily circumvent these RNA inhibitors by creating mutations at the target sequence regions (Lee and Rossi, 2004). On the other hand, the present strategy using MazF targets abundant ACA sequences in HIV-1 RNA (>240), so that it is not possible for HIV-1 to escape from MazF attack by mutations. Furthermore, because MazF has no homology to any mammalian ribonucleases, MazF mRNA interferase activity cannot be inhibited by ribonuclease inhibitors existing in mammalian cells.

In summary, the use of MazF appears to be a novel and highly effective tool for anti-HIV gene therapy. It is effectively able to suppress HIV-1 replication, preventing the emergence of mutated HIV-1. Importantly, MazF induction by invading HIV-1 shows little toxicity to host cells while it efficiently suppresses HIV-1 replication. Specific inhibition of HIV-1 replication by MazF without affecting cell growth is the key feature of MazF-based HIV-1 gene therapy. This may be the first step for RNase-based HIV-1 gene therapy with efficacy *in vitro*. The feasibility of the MazF-based *ex vivo* gene therapy may be verified using autologous CD4+ T lymphocytes from HIV-1 patients. To use our *mazF* vector system for gene therapy, its safety has to be critically evaluated and it should not have any negative impacts on T-cell function. For example, it needs to be shown that there is no alteration in the secretion of functionally important cytokines even though it was observed that MazF expression in HIV-infected CD4+ T cells does not inhibit cell growth. We are currently addressing this question.

### Acknowledgments

The authors thank Dr. Keith A. Reimann of Harvard Medical School and Dr. Tomoyuki Miura of Kyoto University for providing the SHIV 89.6P. The authors also thank Dr. Koich Inoue of Takara Bio Inc. for his critical reading of the manuscript.

### Author Disclosure Statement

No competing financial interests exist.

### References

Agarwal, S., Nikolai, B., Yamaguchi, T., Lech, P., and Somia N.V. (2006). Construction and use of retroviral vectors encoding the toxic gene barnase. Mol. Ther. 14, 555–563.

Berkhout, B., Silverman, R.H., and Jeang, K.T. (1989). Tat transactivates the human immunodeficiency virus through a nascent RNA target. Cell 59, 273–282.

Kim, S., Ikeuchi, K., Byrn, R., Groopman, J., and Baltimore, D. (1989). Lack of a negative influence on viral growth by the nef gene of human immunodeficiency virus type 1. Proc. Natl. Acad. Sci. U.S.A. 86, 9544–9548.

Lee, J.T., Yu, S.S., Han, E., Kim, S., and Kim, S. (2004). Engineering the splice acceptor for improved gene expression and viral titer in an MLV-based retroviral vector. Gene Ther. 11, 94–99.

Lee, N.S., and Rossi, J.J. (2004). Control of HIV-1 replication by RNA interference. Virus Res. 102, 53–58.

Levine, B.L., Humeau, L.M., Boyer, J., MacGregor, R.R., Rebello, T., Lu, X., Binder, G.K., Slepushkin, V., Lemiale, F., Mascola, J.R., Bushman, F.D., Dropulic, B., and June, C.H. (2006). Gene transfer in humans using a conditionally replicating lentiviral vector. Proc. Natl. Acad. Sci. U.S.A. 103, 17372–17377.

Miyake, A., Ibuki, K., Enose, Y., Suzuki, H., Horiuchi, R., Motohara, M., Saito, N., Nakasone, T., Honda, M., Watanabe, T., Miura, T., and Hayami, M. (2006). Rapid dissemination of a pathogenic simian/human immunodeficiency virus to systemic organs and active replication in lymphoid tissues following intrarectal infection. J. Gen. Virol. 87, 1311–1320.

Morris, K.V., and Rossi, J.J. (2006). Lentivirus-mediated RNA interference therapy for human immunodeficiency virus type 1 infection. Hum. Gene Ther. 17, 479–486.

Nariya, H., and Inouye, M. (2008). MazF, an mRNA interferase, mediates programmed cell death during multicellular Myxococcus development. Cell 132, 55–66.

Reimann, K.A., Li, J.T., Voss, G., Lekutis, C., Tenner-Racz, K., Racz, P., Lin, W., Montefiori, D.C., Lee-Parritz, D.E., Lu, Y., Collman, R.G., Sodroski, J., and Letvin, N.L. (1996). An env gene derived from a primary human immunodeficiency virus type 1 isolate confers high in vivo replicative capacity to a chimeric simian/human immunodeficiency virus in rhesus monkeys. J. Virol. 70, 3198–3206.

Saxena, S.K., Gravell, M., Wu, Y.N., Mikulski, S.M., Shogen, K., Ardelt, W., and Youle, R.J. (1996). Inhibition of HIV-1 production and selective degradation of viral RNA by an amphibian ribonuclease. J. Biol. Chem. 271, 20783–20788.

Shimazu, T., Degenhardt, K., Nur-E-Kamal, A., Zhang, J., Yoshida, T., Zhang, Y., Mathew, R., White, E., and Inouye, M. (2007). NBK/BIK antagonizes MCL-1 and BCL-XL and activates BAK-mediated apoptosis in response to protein synthesis inhibition. Genes Dev. 21, 929–941.

Silverman, R.H. (2003). Implications for RNase L in prostate cancer biology. Biochemistry 42, 1805–1812.

Verzeletti, S., Bonini, C., Marktel, S., Nobili, N., Ciceri, F., Traversari, C., and Bordignon, C. (1998). Herpes simplex virus thymidine kinase gene transfer for controlled graft-versus-host disease and graft-versus-leukemia: clinical follow-up and improved new vectors. Hum. Gene Ther. 9, 2243–2251.

Yamaguchi, Y., and Inouye, M. (2009). mRNA interferases, sequence-specific endoribonucleases from the toxin-antitoxin systems. Prog. Mol. Biol. Transl. Sci. 85, 467–500.

Yu, S.F., von Rüden, T., Kantoff, P.W., Garber, C., Seiberg, M., Rüther, U., Anderson, W.F., Wagner, E.F., and Gilboa, E.

(1986). Self-inactivating retroviral vectors designed for transfer of whole genes into mammalian cells. Proc. Natl. Acad. Sci. U.S.A. 83, 3194–3198.

Yu, S.S., Han, E., Hong, Y., Lee, J.T., Kim, S., and Kim, S. (2003). Construction of a retroviral vector production system with the minimum possibility of a homologous recombination. Gene Ther. 10, 706–711.

Zhang, Y., Zhang, J., Hoeflich, K.P., Ikura, M., Qing, G., and Inouye, M. (2003). MazF cleaves cellular mRNAs specifically at ACA to block protein synthesis in *Escherichia coli*. Mol. Cell 12, 913–923.

Zhu, L., Zhang, Y., The, J.S., Zhang, J., Connell, N., Rubin, H., and Inouye, M. (2006). Characterization of mRNA interferases from Mycobacterium tuberculosis. J. Biol. Chem. 281, 18638–18643.

Zhu, L., Inoue, K., Yoshizumi, S., Kobayashi, H., Zhang, Y., Ouyang, M., Kato, F., Sugai, M., and Inouye, M. (2009). *Staphylococcus aureus* MazF specifically cleaves a pentad sequence, UACAU, which is unusually abundant in the mRNA for pathogenic adhesive factor SraP. J. Bacteriol. 191, 3248–3255.

Address correspondence to:
*Dr. Ikunoshin Kato*
*Center for Cell and Gene Therapy*
*Takara Bio Inc.*
*Seta 3-4-1*
*Otsu, Shiga*
*520-2193, Japan*

*E-mail:* ikukatiku@zeus.eonet.ne.jp

*Dr. Masayori Inouye*
*Department of Biochemistry*
*Robert Wood Johnson Medical School*
*675 Hoes Lane*
*Piscataway, NJ 08854, USA*

*E-mail:* inouye@umdnj.edu

Received for publication January 5, 2010;
accepted after revision July 22, 2010.

Published online: July 22, 2010.

J. Comp. Path. 2011, Vol. 144, 204–211

Available online at www.sciencedirect.com

ScienceDirect

ELSEVIER
www.elsevier.com/locate/jcpa

SHORT PAPER

# Periventricular Leucomalacia (PVL)-like Lesions in Two Neonatal Cynomolgus Monkeys (*Macaca fascicularis*)

**S. Okabayashi*,†, K. Uchida‡, H. Nakayama‡, C. Ohno*, K. Hanari*, I. Goto* and Y. Yasutomi†**

** Corporation for Production and Research of Laboratory Primates, Hachimandai 1-1, Tsukuba-shi, Ibaraki 305-0843, † Tsukuba Primate Research Center, National Institute of Biomedical Innovation, Hachimandai 1-1, Tsukuba-shi, Ibaraki 305-0843 and ‡ Laboratory of Veterinary Pathology, Graduate School of Agricultural and Life Sciences, The University of Tokyo, Yayoi 1-1-1, Bunkyo-ku, Tokyo 113-8657, Japan*

**Summary**

Periventricular leucomalacia (PVL) is a lesion of immature cerebral white matter that occurs in the perinatal period. In man, PVL is the predominant form of brain injury and a cause of cerebral palsy and cognitive deficits in premature infants. PVL affects fetuses and newborns, particularly those who have undergone oxygen deprivation as may occur in premature birth. Many clinical and pathological studies of PVL have been performed in man, but there is no clear definition of PVL in animals. A few spontaneous PVL-like cases in puppies or experimental cases in other animal species have been reported. The present study reports the histopathological and immunohistochemical features of PVL-like lesions in two neonatal cynomolgus monkeys. In both cases, there was cerebral white matter necrosis with marked infiltration of lipid-laden phagocytes and a reduction of neurons in the cerebral cortex. In case 1 there was extensive cavitation of the cerebral white matter. In case 2 there was reactive astrocytosis associated with a decrease in oligodendroglial cells and a decrease in cerebral white matter myelin. To our knowledge, this is the first report of PVL-like leucoencephalomalacia in non-human primates.



*Keywords:* cynomolgus monkey; histopathology; immunohistochemistry; periventricular leucomalacia

Cerebral white matter injury in premature human infants is a problem of major clinical importance. These injuries take the form of multiple different lesions including intraventricular haemorrhage, post-haemorrhagic hydrocephalus and periventricular leucomalacia (PVL). PVL is the major form of cerebral white matter injury that affects premature infants and is associated with the subsequent development of cerebral palsy. The characteristic lesion of PVL consists of focal periventricular necrosis, with subsequent cyst formation and more diffuse cerebral white matter injury (Khwaja and Volpe, 2008). Although the pathogenesis of PVL remains to be completely elucidated, it is likely that the necrosis of white matter relates to impaired perfusion resulting from hypoxia–ischaemia (Khwaja and Volpe, 2008). An alternative hypothesis proposes that the lesions result from intrauterine infection with direct toxic effects on fetal oligodendrocytes and astrocytes by cytokines (Damman and Levinton, 1997). Risk factors for PVL include prematurity, asphyxia, respiratory distress, septicaemia, chorioamnionitis, arterial hypotension and hypocarbia (Resch *et al.*, 2004).

There is no clear definition of PVL in animals; however, animal models are necessary for understanding the mechanism of PVL in man. Although a few spontaneous PVL-like cases have been described in puppies (Rentmeister *et al.*, 2004) and several experimental cases (Young *et al.*, 1982; Levison *et al.*, 2001; Brazel *et al.*, 2004) have been reported, no model

Correspondence to: S. Okabayashi · e-mail: okarin@primate.or.jp ·.

0021-9975/$ - see front matter
doi:10.1016/j.jcpa.2010.06.006

reliably replicates all aspects of human PVL. Non-human primates have motor functions and cognitive abilities similar to man and have therefore become increasingly important as experimental models for the study of human central nervous system (CNS) disease. However, PVL-like disease has yet to be described in non-human primates. Here, we report two spontaneously arising cases of PVL-like lesions in neonatal cynomolgus monkeys (*Macaca fascicularis*).

Case 1 was a neonatal female cynomolgus monkey from the Tsukuba Primate Research Center (TPRC) that was delivered by caesarean section at 163 days of gestation as the mother had difficulties in parturition associated with profuse vaginal haemorrhage. The neonate did not breathe for several minutes, but was successfully resuscitated. The body weight of the monkey was 290 g and the animal was artificially nursed. Three days later, paralysis of the limbs was observed and the monkey became progressively debilitated due to insufficient sucking of milk. Despite treatment with subcutaneous infusion of 5% glucose solution and emergency medical care, the monkey died naturally 21 days after birth.

Case 2 was a neonatal male cynomolgus monkey born in the TPRC 16 days prior to the expected date of confinement. The mother rejected the neonate and artificial nursing was conducted. Despite the preterm birth, the body weight of this monkey was 290 g (the average weight of neonatal cynomolgus monkeys in the TPRC is approximately 300–350 g). The next day, paralysis of the limbs was observed and the monkey could not suck sufficient milk. Because this monkey had abnormal breath sounds 3 days after birth, the veterinarian continued treatment with subcutaneous infusion of 5% glucose solution and antibiotics. However, the monkey died naturally 7 days after birth.

Necropsy examination was performed in each case. Tissues were fixed in 10% neutral buffered formalin, processed routinely and embedded in paraffin wax. Sections (3 μm) were stained with haematoxylin and eosin (HE). For immunohistochemistry (IHC), dewaxed sections were pretreated with $H_2O_2$ 0.5% in methanol and then subjected to antigen retrieval by immersion in citric acid buffer (pH 6.0) and heating in an autoclave for 10 min at 121°C. Sections were then incubated free floating in primary antibody solution overnight at 4°C. Primary antibodies were mouse monoclonal antibodies specific for glial fibrillary acidic protein (GFAP, clone LF2, Dako, Glostrup, Denmark; 1 in 200 dilution), CD68 (clone KP1, Dako; 1 in 100 dilution), vimentin (clone 3B4, Dako; 1 in 200 dilution), neurofilament (NF, clone 2F11, Dako; 1 in 100 dilution) and active-caspase-3 (Cas3; Chemicon, Temecula, California; 1 in 100 dilution). Following brief washes with buffer, the sections were incubated sequentially with polymer immunocomplex (Dako) for 30 min. Immunoreactive elements were 'visualized' by treating the sections with 3, 3′-diaminobenzidine tetroxide (Dojin Kagaku, Kunamoto, Japan) followed by counterstaining with haematoxylin.

For double immunolabelling, sections were dewaxed and then stained with 1% Sudan black B to reduce autofluorescence. Following brief washes, sections were incubated free floating overnight at 4°C in solutions containing mouse monoclonal antibody for myelin basic protein (MBP; Chemicon; 1 in 500 dilution) and rabbit polyclonal antibody specific for oligodendrocytes (olig2; IBL, Takasaki, Gunma, Japan; 1 in 500 dilution). Sections were then incubated with AlexaFluor 488-conjugated goat anti-mouse IgG (Invitrogen, Carlsbad, California; 1 in 1,000 dilution) and AlexaFluor 555-conjugated goat anti-rabbit IgG (Invitrogen; 1 in 1,000 dilution) for 1 h at room temperature. The sections were examined with a Digital Eclipse C1 confocal microscope (Nikon, Kanagawa, Japan). Neonatal monkey brain sections (0-day-old animals) were used as normal controls.

Grossly, the neonatal monkeys were emaciated, dehydrated and had pale mucous membranes. Both limbs and the tail had a decreased range of motion and atrophy of limb muscles was observed in each case. Both tracheas were filled with mucus mixed with milk. The lungs were oedematous and hyperaemic and there were several small white nodules (2–3 mm diameter) in all pulmonary lobes in case 2. In case 1, an excessive quantity of cerebrospinal fluid (CSF) had accumulated in the cranial cavity and the volume of the cerebrum appeared reduced. After formalin fixation, cross sections of the cerebrum in case 1 revealed the presence of marked cavitation of the white matter and atrophy of the cortical region (Fig. 1A), whereas multiple foci of softening of the white matter were found in cross sections of the cerebrum in case 2 (Fig. 1B).

Microscopically, in case 1 areas of cavitation or foci of liquefactive necrosis were widespread with loss of all cellular elements from white matter to deep gray matter, with many lipid-filled phagocytes aggregated within the necrotic foci (Fig. 2A). Residual cerebral cortex showed marked reduction in the number of neural cells. The lateral ventricle was enlarged, with hyperaemia of the choroid plexus, and the ependymal layers showed glial cell infiltration and partial exfoliation. Glial cell infiltration, glial nodules and aggregation of lipid-filled phagocytes with formation of cholesterol clefts were found in the periventricular regions of the lateral ventricle. However, the

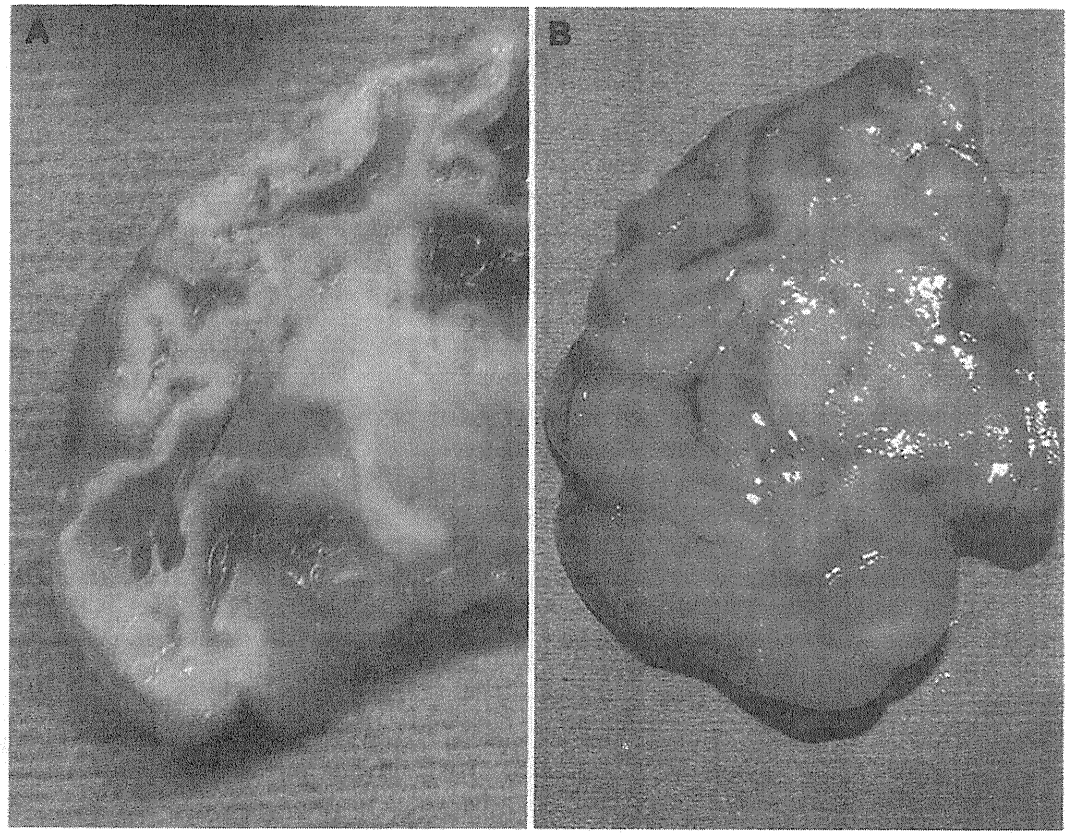


Fig. 1. (A) Cerebrum of a 21-day-old cynomolgus monkey (case 1). Marked cavitation of the white matter and atrophy of the cortical region are present in the temporal lobe. (B) Cerebrum in a 7-day-old cynomolgus monkey (case 2). Multiple foci of white matter softening are present in the temporal lobe.

periventricular regions and ependymal layers of the third ventricle appeared to be largely normal, except for a slight infiltration of glial cells. In case 2, the cerebrum showed massive liquefactive necrosis, with infiltration of lipid-filled phagocytes bilaterally in the temporal white matter and particularly in the periventricular areas of the lateral ventricle. Furthermore, there was diffuse reactive astrocytosis with gemistocytes (Fig. 3A) in various white matter areas and focally in the temporal deep gray matter. The density of neuronal cells was significantly reduced in the lesional sites. Periventricular areas of the third ventricle and thalamus also showed a decrease in neurons infiltration of lipid-filled phagocytes and astrocytosis. Examination of the brainstem, cerebellum, spinal cord and optic nerves did not reveal any abnormalities in either case.

In case 1, immunohistochemical labelling for expression of GFAP revealed apparent proliferation of glial fibrils in the cerebral cortex around cavitations or foci of liquefactive necrosis consistent with glial scar formation (Fig. 2B). In case 2, gemistocytes in the cerebral white matter displayed strong cytoplasmic immunoreactivity for GFAP (Fig. 3A). Immature astrocytes with narrow cytoplasm and long processes were immunolabelled for GFAP and vimentin (Fig. 3B) in the cerebral cortex and the cerebral white matter. Lipid-filled phagocytes in necrotic foci displayed granular cytoplasmic immunoreactivity for CD68 in both cases (Fig. 2A). Neurons displaying immunoreactivity for NF were significantly reduced in number in each case. Both cases were negative for Cas3 expression, suggesting that the lesions were a result of necrosis rather than apoptosis. Double immunohistochemical labelling with anti-MBP and anti-olig2 was also performed. In normal neonatal monkey brains, some oligodendroglial cells and many myelin sheaths were observed in the white matter (Fig. 4). In contrast, the white matter in case 2 showed a marked decrease in oligodendroglial cells and myelin sheaths (Fig. 4). The white matter in case 1 was unlabelled due to loss of all cellular elements within the areas of cavitation.

In case 1, the lung showed alveolar collapse with proliferation of type II alveolar epithelial cells (AEC II) and infiltration of macrophages into the alveolar space. In case 2, the lung showed severe diffuse pneumonia with infiltration of neutrophils and macrophages into the alveolar space and exfoliation of the alveolar epithelium.

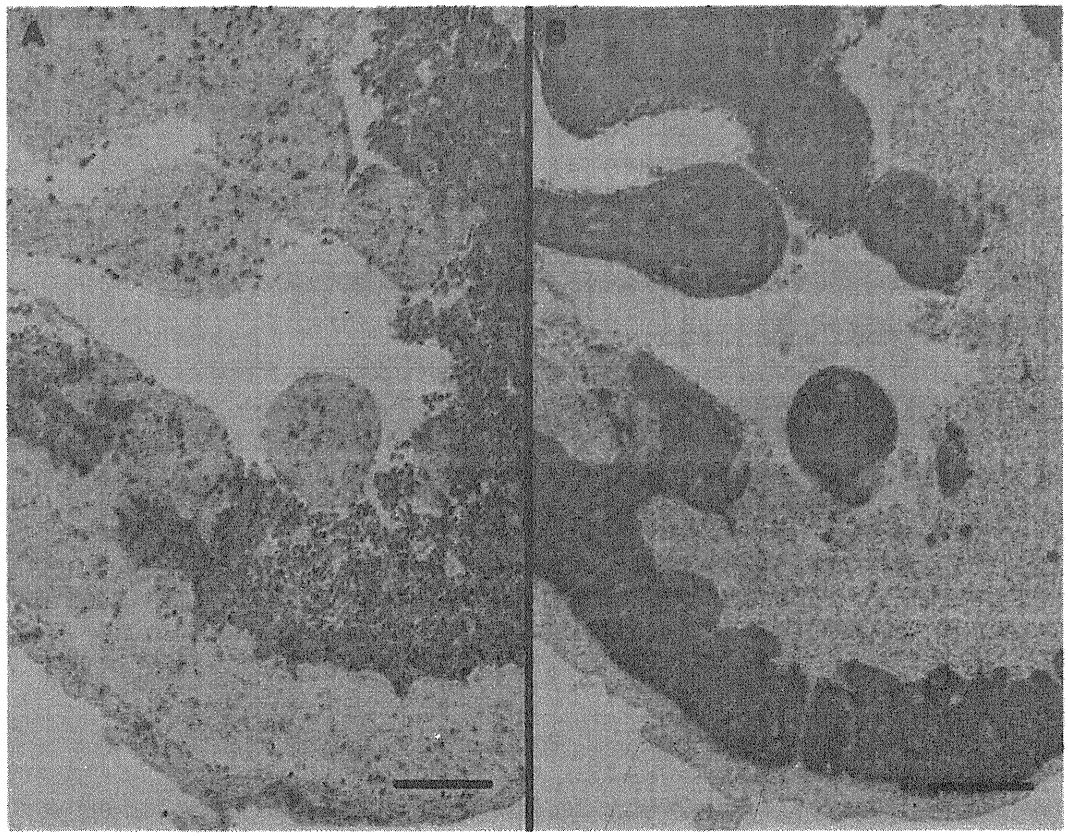


Fig. 2. Cerebrum of a 21-day-old cynomolgus monkey (case 1). (A) There is cavitation or foci of liquefactive necrosis with loss of all cellular elements from white matter to deep gray matter, with aggregation of many lipid-filled phagocytes expressing CD68 in the necrotic foci. IHC. Bar, 200 μm. (B) There is apparent proliferation of glial fibrils around these areas of cavitation or liquefactive necrosis. IHC. Bar, 200 μm.

Some colonies of gram-positive bacteria with morphology consistent with *Staphylococcus* were also observed within the white nodules in the lungs. Additionally, gastric contents, including milk, were found in the trachea of both cases. Atrophy of femoral muscles was observed with proliferation of stromal connective tissue in each case, and this change was particularly severe in case 1. The sciatic nerves of both monkeys appeared almost normal, but there was proliferation of surrounding perineural connective tissue.

Brain injury in the premature human infant consists of multiple lesions, principally germinal intraventricular haemorrhage, post-haemorrhagic hydrocephalus and PVL (Volpe, 2003). PVL refers to injury of the cerebral white matter that occurs with characteristic distribution and consists of focal periventricular necrosis with subsequent cyst formation (cystic PVL) and more diffuse cerebral white matter necrosis with subsequent glial scaring (non-cystic PVL). A third form of cerebral white matter abnormality (the third form of PVL) consists of diffuse astrogliosis without necrosis (Khwaja and Volpe, 2008). PVL is the major form of brain white matter injury that affects premature human infants and is associated with subsequent development of cerebral palsy, intellectual impairment and visual disturbances. There is currently no specific therapy for PVL (Pierson *et al.*, 2007). The diagnostic hallmarks of PVL are periventricular echodensities or cysts detected by cranial ultrasonography (Deng *et al.*, 2008). Two major factors appear to be involved in the development of PVL. The first involves fetal or neonatal hypoxia–ischaemia that can be a consequence of reduced blood flow to the umbilicus, uterus or placenta in the prenatal or perinatal period. Recent studies suggest that a disturbance of circulation, such as severe hypotension, or cardiogenic shock in preterm infants, such as caused by severe perinatal asphyxia, plays a decisive role in the formation of PVL-lesions (Shankaran *et al.*, 2006; Khwaja and Volpe, 2008). Moreover, experimental studies in which hypoxia is induced artificially have been also conducted in animals for exploration of the pathophysiology of PVL (Painter, 1995; Kohlhauser *et al.*, 2000). Anatomically, early in development, the deep penetrating arteries of the middle cerebral artery that supply the periventricular white matter lack the

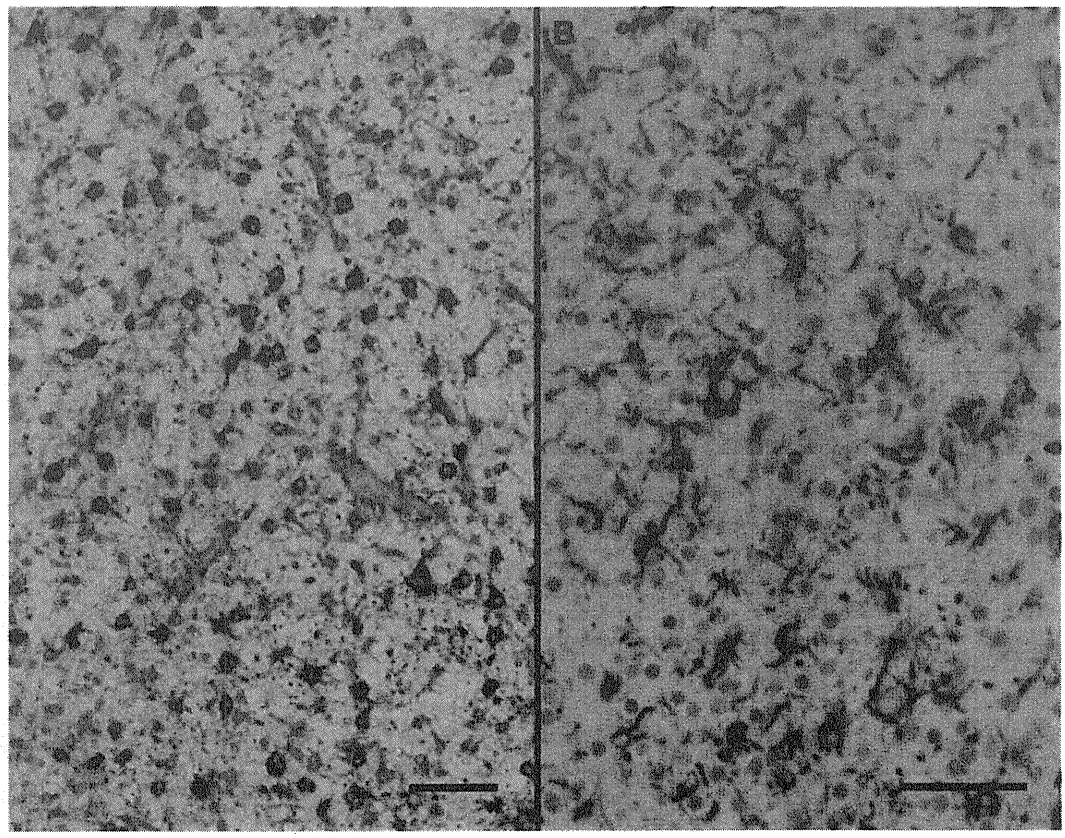

Fig. 3. Cerebrum of a 7-day-old cynomolgus monkey (case 2). (A) Large numbers of reactive astrocytes are present in the cerebral white matter. The cytoplasm of these cells labels for expression of GFAP, an astrocyte-specific marker. IHC. Bar, 50 μm. (B) Premature astrocytes are also present in the cerebral cortex. The narrow cytoplasm and long processes of these cells were immunolabelled for expression of vimentin. IHC. Bar, 50 μm.

vascular anastomoses that help maintain perfusion during periods of hypotension (Takashima *et al.*, 1978; Rorke, 1992; Inage *et al.*, 2000). Therefore, as cerebral autoregulation begins to fail following severe hypotension in neonatal infants, particularly in preterm infants, blood flow is selectively impaired and initially in the white matter of the periventricular region. Furthermore, there is recent evidence that the brain of sick preterm infants often shows impaired cerebrovascular autoregulation in response to change in blood pressure (Soul *et al.*, 2007). This selective hypoperfusion of cerebral white matter during severe hypotension provides a mechanistic explanation for the pathogenesis of PVL. Meanwhile, microglia are activated by the release of reactive oxygen species (ROS) and reactive nitrogen species (RNS), which may mediate cell death. The reactive astrocytes in diffuse lesions could also contribute to the formation of RNS. The release of ROS and RNS by microglia seems likely to result in death of premyelinating oligodendrocytes (pre-OLs) or prevent pre-OLs from differentiating to mature myelin-producing cells in the injured cerebral white matter (Volpe, 2003; Khwaja and Volpe, 2008).

The second major factor contributing to the development of PVL is thought to be maternal intrauterine (or neonatal) infection and fetal (or neonatal) systemic inflammation. Increasing numbers of studies have implicated intrauterine infection in the genesis of PVL. Recent investigations have shown that intravenous injection of the bacterial endotoxin lipopolysaccharide (LPS) can produce selective white matter injury in the neonatal CNS (Paintlia *et al.*, 2008), whereas induction of intrauterine infection can produce diffuse glial cell death and cavitation in fetal white matter (Sherwin and Fern, 2005). The secretion of proinflammatory cytokines such as interleukin (IL)-1, IL-6, and tumor necrosis factor (TNF)-α is known to be toxic to the developing fetal brain (Damman and Levinton, 1997) and may lead to astrogliosis affecting the maturation of myelin-forming oligodendrocytes (Leviton and Gilles, 1996).

The gestation period of the cynomolgus monkey averages 165 days in the TPRC. Case 1 was born on day 163 of gestation and was thus of normal gestational age; however, this animal suffered from a period of asphyxia due to perinatal dystocia. Perinatal asphyxia results from oxygen deprivation that may

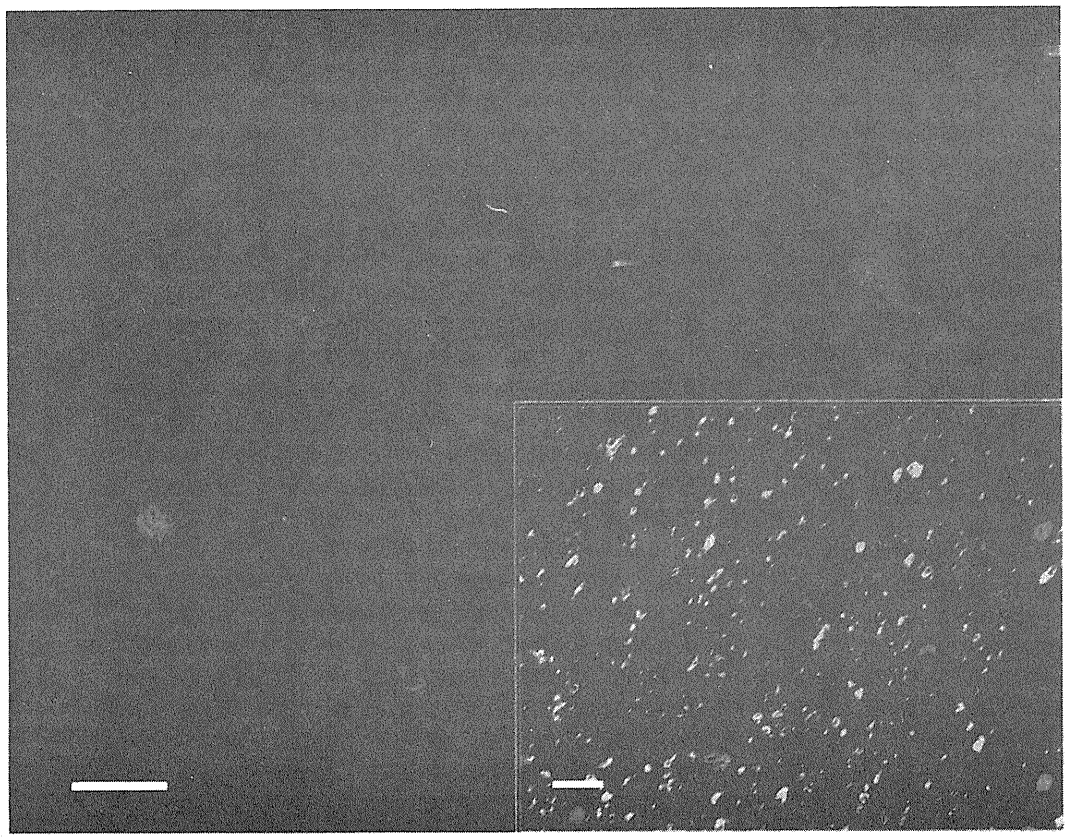

Fig. 4. Cerebrum of a 7-day-old cynomolgus monkey (case 2). Sections were double labelled with antibodies specific for MBP (green) and olig2 (red). There is reduction in cells expressing olig2 and almost no expression of MBP in the cerebral white matter. IHC. Bar, 10 μm. Inset: cerebrum of a normal 0-day-old cynomolgus monkey double labelled as above (control). Within the white matter, oligodendroglial cells express olig2 and many myelin sheaths express MBP. IHC. Bar, 10 μm.

cause harm to the neonatal infant. The condition occurs most commonly due to a drop in maternal blood pressure or interference with blood flow to the brain of the infant during delivery. This was likely to have been the aetiology of the lesions observed in the brain of case 1.

Case 2 was born 16 days before the expected date of confinement. Although PVL may occur in term infants, the injury is more common in premature infants, especially those born between 26 and 34 weeks of gestation (Locatelli *et al.*, 2005). The brain injury in preterm infants is mainly due to the oxidative stress placed on the neonate during delivery (Robles *et al.*, 2001; Haynes *et al.*, 2005), the immaturity of the developing nervous system, and the immaturity of the cerebrovascular supply (Khwaja and Volpe, 2008). Robles *et al.* (2001) investigated the concentration of hydroperoxides, which are measures of oxidative stress. These authors demonstrated that full-term neonates had levels of hydroperoxides that dropped sharply in the first few hours following birth. However, in premature infants the concentration of hydroperoxides remained at near birth levels for as long as a week and at dangerously high levels for even longer. Therefore, preterm neonates are at risk of free-radical injury during this period. In addition to these underlying factors, hypoxia–ischaemia can lead to more free-radical production, which can then damage the pre-OLs (Yoshida-Shuto *et al.*, 1992; Robles *et al.*, 2001). Thus, case 2 was at risk of a nervous system disorder and was of especially high risk for developing PVL. A genetic susceptibility to PVL has been proposed with cytokine genes acting as risk modifiers (Baier, 2006), but there was no familial association between the two animals of the present report.

Case 1 had marked cavitation with loss of cellular elements in the cerebral white matter. These changes are similar to cystic PVL and the cavitations may be formed by fusion of multiple cystic foci. Case 2 did not show cavitation, despite the presence of diffuse necrosis of the cerebral white matter, astrogliosis, decreased oligodendroglial cells and marked dysmyelination. These changes are similar to non-cystic PVL or the third form of PVL, and dysmyelination must have been caused by a decrease of myelin-producing oligodendrocytes and disturbance of pre-OL maturation.

The pathological differences between the two monkeys may also have been influenced by the duration of ischaemia or other factors such as fetal age or the length of survival. In general, it is said that microglial reactivity is apparent within 24 h, peaks at 7 days and remains present for weeks following the ischaemia. Phenotypic changes in resident astrocytes occur at 24 h, and these cells proliferate between 48 h and 7 days after ischaemia. Over the ensuing weeks and months, astrocytes increase in number and in fibrillary appearance, eventually resulting in a glial scar or cavitation (Cervós-Navarro and Lafuente, 1991; Williams *et al.*, 2007). Case 1 had widespread cavitation and severe glial scarring, while case 2 showed neuronal decrease, infiltration of lipid-filled phagocytes and astrocytosis in the cerebral white matter and the thalamus. The thalamus is commonly affected in premature infants with PVL (Volpe, 2009), therefore the thalamic lesion in case 2 may have been linked to preterm birth. Furthermore, in each case the femoral muscles showed apparent neurogenic atrophy, likely secondary to dysfunction of the cerebral white matter.

Both monkeys had diffuse pulmonary lesions. In case 1, alveolar collapse was observed with proliferation of AEC II. This may have been caused by artificial ventilation and inhalation of highly concentrated oxygen administered as part of the medical care of the animal. Hyperoxia or hypocarbia results in the death of AEC I and subsequent proliferation of AEC II that differentiate to AEC I to replace the injured or dead AECs during the recovery stages (Takemura and Akamatsu, 1987). Case 2 showed severe purulent alveolar pneumonia with bacterial infection. This bacterial pneumonia may have been due to compromise of the immune system or decreased strength in this premature infant. Both tracheas were filled with a mixture of milk and mucus, suggesting that the animals may have terminally aspirated gastric contents.

Criteria for PVL in animals have not been defined, but the clinical and pathological features of our cases were very similar to those of PVL in man. TPRC has a large-scale breeding colony of experimental cynomolgus monkeys, with about 200 births each year. However, these are the first cases experienced in the TPRC and the first from any primate centre. Future cases should also be subject to ultrasonographic or magnetic resonance imaging investigation. Brain injury in premature infants has an enormous importance to public health because of the large number of such infants who survive with serious neurodevelopmental disability, including major cognitive deficits and motor disability. Because man and monkeys are very similar in anatomy, motor function and cognitive ability, monkeys are favoured as non-human primate models for the study of post-injury changes in the CNS. These spontaneously arising cases in non-human primates will contribute greatly to understanding the pathophysiology of PVL and to the development of an effective therapy for PVL or cerebral palsy.

## Acknowledgments

This study was supported by the Tsukuba Primate Research Center, National Institute of Biomedical Innovation, Japan.

## References

Baier RJ (2006) Genetics of perinatal brain injury in the preterm infant. *Frontiers in Biosciences*, **11**, 1371–1387.

Brazel CY, Rosti RT, Boyce S, Rothstein RP, Levison SW (2004) Perinatal hypoxia/ischemia damages and depletes progenitors from the mouse subventricular zone. *Developmental Neuroscience*, **26**, 266–274.

Cervós-Navarro J, Lafuente JV (1991) Traumatic brain injuries: structural changes. *Journal of Neurological Science*, **103**, S3–S14.

Damman O, Levinton A (1997) Maternal intrauterine infection, cytokines, and brain damage in the preterm newborn. *Pediatric Research*, **42**, 1–8.

Deng W, Pleasure J, Pleasure D (2008) Progress in periventricular leukomalacia. *Archives of Neurology*, **65**, 1291–1295.

Haynes RL, Baud O, Li J, Kinney HC, Volpe JJ *et al.* (2005) Oxidative and nitrative injury in periventricular leukomalacia: a review. *Brain Pathology*, **15**, 225–233.

Inage YW, Itoh M, Takashima S (2000) Correlation between cerebrovascular maturity and periventricular leukomalacia. *Pediatric Neurology*, **22**, 204–208.

Khwaja O, Volpe JJ (2008) Pathogenesis of cerebral white matter injury of prematurity. *Archives of Disease in Childhood. Fetal and Neonatal Edition*, **93**, 153–161.

Kohlhauser C, Mosgöller W, Höger H, Lubec B (2000) Myelination deficits in brain of rats following perinatal asphyxia. *Life Sciences*, **67**, 2355–2368.

Levison SW, Rothstein RP, Romanko MJ, Snyder MJ, Meyers RL *et al.* (2001) Hypoxia/ischemia depletes the rat perinatal subventricular zone of oligodendrocyte progenitors and neural stem cells. *Developmental Neuroscience*, **23**, 234–247.

Leviton A, Gilles F (1996) Ventriculomegaly, delayed myelination, white matter hypoplasia, and 'periventricular' leukomalacia: how are they related? *Pediatric Neurology*, **15**, 127–136.

Locatelli A, Ghidini A, Paterlini G, Patanè L, Doria V *et al.* (2005) Gestational age at preterm premature rupture of membranes: a risk factor for neonatal white matter damage. *American Journal of Obstetrics and Gynecology*, **193**, 947–951.

Painter MJ (1995) Animal models of perinatal asphyxia: contributions, contradictions, clinical relevance. *Seminars in Pediatric Neurology*, **2**, 37–56.

Paintlia MK, Paintlia AS, Contreras MA, Singh I, Singh AK (2008) Lipopolysaccharide-induced

peroxisomal dysfunction exacerbates cerebral white matter injury: attenuation by N-acetyl cysteine. *Experimental Neurology*, **210**, 560–576.

Pierson CR, Folkerth RD, Billiards SS, Trachtenberg FL, Drinkwater ME *et al.* (2007) Gray matter injury associated with periventricular leukomalacia in the premature infant. *Acta Neuropathology*, **114**, 619–631.

Rentmeister K, Schmidbauer S, Hewicker-Trautwein M, Tipold A (2004) Periventricular and subcortical leukoencephalopathy in two dachshund puppies. *Journal of Veterinary Medicine Series A: Physiology, Pathology and Clinical Medicine*, **51**, 327–331.

Resch B, Jammernegg A, Vollaard E, Maurer U, Mueller WD *et al.* (2004) Preterm twin gestation and cystic periventricular leucomalacia. *Archives of Disease in Childhood. Fetal and Neonatal Edition*, **89**, F315–320.

Robles R, Palomino N, Robles A (2001) Oxidative stress in the neonate. *Early Human Development*, **65**, S75–S81.

Rorke LB (1992) Anatomical features of the developing brain implicated in pathogenesis of hypoxic-ischemic injury. *Brain Pathology*, **2**, 211–221.

Shankaran S, Langer JC, Kazzi SN, Laptook AR, Walsh M (2006) Cumulative index of exposure to hypocarbia and hyperoxia as risk factors for periventricular leukomalacia in low birth weight infants. *Pediatrics*, **118**, 1654–1659.

Sherwin C, Fern R (2005) Acute lipopolysaccharide-mediated injury in neonatal white matter glia: role of TNF-alpha, IL-1beta, and calcium. *Journal of Immunology*, **175**, 155–161.

Soul JS, Hammer PE, Tsuji M, Saul JP, Bassan H *et al.* (2007) Fluctuating pressure-passivity is common in the cerebral circulation of sick premature infants. *Pediatric Research*, **61**, 467–473.

Takashima S, Armstrong DL, Becker LE (1978) Subcortical leukomalacia. Relationship to development of the cerebral sulcus and its vascular supply. *Archives of Neurology*, **35**, 470–472.

Takemura T, Akamatsu H (1987) Ultrastructural study on the pulmonary parenchyma of the neonates following prolonged mechanical ventilation. *Acta Pathologica Japonica*, **37**, 1115–1126.

Volpe JJ (2003) Cerebral white matter injury of the premature infant – more common than you think. *Pediatrics*, **112**, 176–180.

Volpe JJ (2009) Brain injury in premature infants: a complex amalgam of destructive and developmental disturbances. *Lancet Neurology*, **8**, 110–124.

Williams AJ, Wei HH, Dave JR, Tortella FC (2007) Acute and delayed neuroinflammatory response following experimental penetrating ballistic brain injury in the rat. *Journal of Neuroinflammation*, **2**, 4–17.

Yoshida-Shuto H, Yasuhara A, Kobayashi Y (1992) Cerebral blood flow velocity and failure of autoregulation in neonates: their relation to outcome of birth asphyxia. *Neuropediatrics*, **23**, 241–244.

Young RS, Hernandez MJ, Yagel SK (1982) Selective reduction of blood flow to white matter during hypotension in newborn dogs: a possible mechanism of periventricular leukomalacia. *Annals of Neurology*, **12**, 445–448.

[ *Received, January 23rd, 2010*
*Accepted, June 27th, 2010* ]

frontiers in
MICROBIOLOGY

ORIGINAL RESEARCH ARTICLE
published: 07 December 2011
doi: 10.3389/fmicb.2011.00240

# Long-term persistent GBV-B infection and development of a chronic and progressive hepatitis C-like disease in marmosets

**Yuki Iwasaki[1,2†], Ken-ichi Mori[3†], Koji Ishii[4], Noboru Maki[3], Sayuki Iijima[1], Tomoyuki Yoshida[5], Sachi Okabayashi[6], Yuko Katakai[6], Young-Jung Lee[1], Akatsuki Saito[5], Hiromi Fukai[3], Nobuyuki Kimura[1], Naohide Ageyama[1], Sayaka Yoshizaki[4], Tetsuro Suzuki[4], Yasuhiro Yasutomi[1], Tatsuo Miyamura[4], Mari Kannagi[2] and Hirofumi Akari[1,5]***

[1] Tsukuba Primate Research Center, National Institute of Biomedical Innovation, Tsukuba, Japan
[2] Department of Immunotherapeutics, Graduate School of Medicine and Dentistry, Tokyo Medical and Dental University, Tokyo, Japan
[3] Advanced Life Science Institute, Wako, Japan
[4] Department of Virology II, National Institute of Infectious Diseases, Tokyo, Japan
[5] Primate Research Institute, Kyoto University, Inuyama, Japan
[6] Corporation for Production and Research of Laboratory Primates, Tsukuba, Japan

***Edited by:***
*Yasuko Yokota, National Institute of Infectious Diseases, Japan*

***Reviewed by:***
*Ikuo Shoji, Kobe University Graduate School of Medicine, Japan*
*Soon B. Hwang, Hallym University, South Korea*

***Correspondence:**
*Hirofumi Akari, Primate Research Institute, Kyoto University, Inuyama 484-8506, Japan.*
*e-mail: akari@pri.kyoto-u.ac.jp*

†*Yuki Iwasaki and Ken-ichi Mori have contributed equally to this work.*

It has been shown that infection of GB virus B (GBV-B), which is closely related to hepatitis C virus, develops acute self-resolving hepatitis in tamarins. In this study we sought to examine longitudinally the dynamics of viral and immunological status following GBV-B infection of marmosets and tamarins. Surprisingly, two of four marmosets but not tamarins experimentally challenged with GBV-B developed long-term chronic infection with fluctuated viremia, recurrent increase of alanine aminotransferase and plateaued titers of the antiviral antibodies, which was comparable to chronic hepatitis C in humans. Moreover, one of the chronically infected marmosets developed an acute exacerbation of chronic hepatitis as revealed by biochemical, histological, and immunopathological analyses. Of note, periodical analyses of the viral genomes in these marmosets indicated frequent and selective non-synonymous mutations, suggesting efficient evasion of the virus from antiviral immune pressure. These results demonstrated for the first time that GBV-B could induce chronic hepatitis C-like disease in marmosets and that the outcome of the viral infection and disease progression may depend on the differences between species and individuals.

**Keywords: GBV-B, HCV, marmoset, tamarin, hepatitis C**

## INTRODUCTION

Among the known viruses, GB virus B (GBV-B) is closely related to hepatitis C virus (HCV), with 25–30% homology at the amino acid level, and is tentatively classified in *Hepacivirus* genus of *Flavivirus* family (Muerhoff et al., 1995; Simons et al., 1995; Ohba et al., 1996). Due to limited epidemiological analyses, the natural host(s) and prevalence of GBV-B have remained to be determined.

Hepatitis C virus is a major causative agent for non-A, non-B hepatitis. HCV is globally disseminated and estimated to be carried by more than 170 million people (Chisari, 2005; Lavanchy, 2009). Most HCV-infected individuals develop chronic liver diseases such as liver cirrhosis and hepatocellular carcinoma (Hoofnagle, 1997; Seeff and Hoofnagle, 2002; Rehermann and Nascimbeni, 2005). Since standard therapy with PEGylated interferon and ribavirin is effective for only about 50% of patients, it is crucial to develop more effective therapeutics (Feld and Hoofnagle, 2005; Melnikova, 2008). The only validated animal model for HCV infection is the chimpanzees. This model has been valuable for determining important aspects of this disease, including the relationship between the virus and the antiviral immune responses of the host and the process of viral pathogenesis (Bukh, 2004; Akari et al., 2009; Boonstra et al., 2009). However, chimpanzees are endangered and present ethical complications and the availability of these experimental animals is severely restricted.

When tamarins (members of the New World monkeys) are infected with GBV-B, they generally develop acute viremia and self-resolving hepatitis as indicated by increases in the levels of serum enzymes such as alanine aminotransferase (ALT) (Bukh et al., 1999; Beames et al., 2000; Beames et al., 2001; Sbardellati et al., 2001; Lanford et al., 2003; Martin et al., 2003; Bright et al., 2004; Jacob et al., 2004; Nam et al., 2004; Kyuregyan et al., 2005; Ishii et al., 2007; Weatherford et al., 2009). Thus, the monkeys have been proposed as a surrogate model of HCV infection of chimpanzee and humans. However, a major hurdle for the development of a monkey-based surrogate model is the difficulties encountered in obtaining chronically infected monkeys that exhibit progression of chronic hepatitis C-like diseases (Martin et al., 2003; Nam et al., 2004; Takikawa et al., 2010).

**Abbreviations:** ALT, alanine aminotransferase; GBV-B, GB virus B; HCV, hepatitis C virus; HE, hematoxylin and eosin; p.i., post infection.

It has recently been shown that marmosets, another member of New World monkeys, are susceptible to GBV-B infection and develop relatively lower levels of acute viremia ($10^5$–$10^8$ copies/ml) as compared with that in tamarins ($10^7$–$10^{10}$ copies/ml) (Lanford et al., 2003; Bright et al., 2004; Woollard et al., 2008; Weatherford et al., 2009), although it remains elusive whether the marmosets could permit persistent GBV-B infection. Considering that the viral loads in the acute phase of experimental HCV infection of chimpanzees that consequently develop persistent infection are generally $10^7$ copies/ml or less (Fernandez et al., 2004; Bukh et al., 2008), it is possible that the lower viral loads in the acute phase is preferable for the establishment of viral persistency. We thus initiated studies of the dynamics of viral and immunological status following GBV-B infection of tamarins and marmosets in a longitudinal follow-up study. We show here for the first time that GBV-B infection produces a chronic and progressive hepatitis C-like disease in marmosets as demonstrated by fibrosis and a recurrent ALT increase and that one of the marmosets experienced acute exacerbation of chronic hepatitis as indicated by piecemeal necrosis and an ALT flare >4 years after infection.

## MATERIALS AND METHODS

### ANIMALS

Adult red-handed tamarins (*Saguinus midas*) and common marmosets (*Callithrix jacchus*) were housed in individual cages at the Tsukuba Primate Research Center. All animal studies were conducted in accordance with the protocols of experimental procedures that were approved by the Animal Welfare and Animal Care Committees of the National Institute of Biomedical Innovation and the National Institute of Infectious Diseases.

### GBV-B INFECTION IN TAMARINS AND MARMOSETS

GBV-B infectious serum obtained from a tamarin ($1.3 \times 10^9$ viral RNA copies per inoculum) was injected into each tamarin and marmoset intrahepatically as previously described (Ishii et al., 2007). We confirmed that the inoculum contained no mutations as compared with the original sequence. Of note, an anti-luciferase siRNA in a cationic liposome formulation was administered to one of the marmosets (Cj05-002) 2 days before the infection, which was performed as previously described (Yokota et al., 2007). Blood samples were periodically collected from the femoral vein of each animal under anesthesia and the plasma samples were evaluated for GBV-B genomic RNA, ALT, and antibodies against GBV-B core and NS3 proteins.

### QUANTIFICATION OF GBV-B GENOMIC RNA

GBV-B RNA was isolated from the plasma samples by using a QIAamp MinElute Virus Spin kit (QIAGEN) and was quantified by real-time PCR using the 5′-exonuclease PCR (TaqMan) assay system (Ishii et al., 2007). The primers 558F [5′-AACGAGCAAAGCGCAAAGTC] and 626R [5′-CATCATGGATACCAGCAATTTTGT] and the probe 579P [5′-FAM-AGCGCGATGCTCGGCCTCGTA-TAMRA] (Beames et al., 2000) were obtained from Sigma-Aldrich. The cutoff value was $10^3$ copies/ml. All the specimens were evaluated in duplicate and the average values were calculated.

### DETECTION OF ANTIBODIES AGAINST GBV-B CORE AND NS3 PROTEINS BY ELISA

Tamarin and marmoset plasma samples were evaluated for anti-GBV-B core and NS3 antibodies by ELISA as described previously (Ishii et al., 2007).

### HISTOPATHOLOGICAL AND IMMUNOHISTOCHEMICAL ANALYSES

Liver samples obtained by necropsy from the GBV-B-infected marmoset were examined histopathologically as previously described (Ishii et al., 2007). For standard histological examination, the sections were subjected to hematoxylin and eosin (HE) staining. Masson's trichrome staining was also performed to estimate the development of fibrosis according to a standard laboratory protocol. To detect the viral protein in tissues, we employed a mouse anti-core monoclonal antibody, 5A10, that we generated. In brief, Mice were immunized with the GBV-B core protein expressed in *E. coli* (Ishii et al., 2007). Hybridoma cells producing an anti-core mAb were screened by both the core-expressing 293T cells and the liver sections of an acutely GBV-B-infected tamarin. Liver samples were fixed in 10% neutral buffered formalin and embedded in paraffin wax. Sections were deparaffinized by pretreating with 0.5% periodic acid and then subjected to antigen retrieval with citric acid buffer and heating in an autoclave for 10 min at 121°C. The sections were then incubated free floating in primary antibody solution (5A10; 1:50 dilution) overnight at 4°C. Following brief washes with wash buffer, the sections were sequentially incubated with a biotinylated goat anti-mouse IgG (1:400 dilution), followed by addition of a streptavidin–biotin–horseradish peroxidase complex (sABC kit; DAKO, Denmark). Immunoreactive elements in the sections were visualized by treatment with 3,3′-diaminobenzidine tetroxide (Dojin Kagaku, Japan), together with counterstaining with hematoxylin.

### DETERMINATION OF THE GBV-B SEQUENCE

Viral RNA was isolated from the plasma of GBV-B-infected marmosets as described above. GBV-B cDNA was synthesized using SuperScript reverse transcriptase III (Invitrogen) with random hexamer primers (Invitrogen). The resulting cDNAs were used to obtain PCR amplification products of lengths of 0.5–1.0 kb, using GBV-B-specific primers and LA-Taq DNA polymerase (TaKaRa). The PCR products were then purified from the gel using a QIA-quick gel extraction kit (QIAGEN), and the purified amplimers were sequenced directly using a CEQ-2000XL analysis system (Beckman) with a DTCS quick start kit and GBV-B-specific primers according to the manufacturer's instructions. Sequence data were analyzed using the Sequencher 4.8 (Gene Codes) and Mac Vector 10.6 (MacVector) software packages. The GenBank accession numbers of the viral genome sequences in each time point are as follows: AB630358, AB630359, and AB630360 for 45, 104, and 135 weeks after infection in Cj05-002; AB630361, AB630362, AB630363, and AB630364 for 33, 88, 141, and 229 weeks after infection in Cj05-004, respectively. Throughout this article, the amino acids are numbered according to the full-length genome sequence of isolate pGBB (GenBank accession number AF179612).

## RESULTS

### GBV-B INFECTION IN TAMARINS AND MARMOSETS

Four tamarins and four marmosets were intrahepatically inoculated with GBV-B and the growth kinetics and pathogenesis of the virus were compared. In tamarins, the peak viral loads in plasma reached $10^9$–$10^{10}$ copies/ml in the acute phase and the viremia was maintained for an average of 3 months in parallel with increases in plasma ALT levels (**Figure 1A**). Antibodies reactive with the viral core and NS3 proteins were developed in all of the tamarins as the plasma viral loads were reduced and the antibody titers reached maximum levels concurrently with the complete loss of detectable viral RNA (**Figure 1A**). In contrast, two of four marmosets infected with GBV-B developed chronic infection while the others exhibited a phenotype similar to that of the tamarins (i.e., subacute clearance of the viremia followed by antibody responses). One exception is that lower plasma viral loads ($10^7$–$10^8$ copies/ml) were observed in the marmosets relative to those of the tamarins (**Figure 1B**). The details of the chronically infected marmosets are described below.

Case 1: Cj05-002 (**Figures 1B** and **2**). The viral RNA was undetectable until week 4 post infection (p.i.) and then gradually increased to a peak at week 18 p.i. ($3 \times 10^7$ copies/ml). Subsequently, this case retained intermittent viremia during the observation period of week 180 p.i., while the intervals between the viremia phases were prolonged. Importantly, the titers of anti-core and anti-NS3 antibodies reached a persistent plateau at 6 months and 1 year p.i., respectively. In addition, ALT levels were recurrently increased without observation of other clinical symptoms.

Case 2: Cj05-004 (**Figures 1B** and **2**). During the acute phase of infection, the level of viremia was relatively low and transient, followed by a 1-year period when the virus was essentially undetectable. Irrespective of the very low viral load, the titer of anti-NS3 but not anti-core antibody steadily increased and reached a plateau at week 42 p.i. Moreover, an occasional but obvious increase in the level of ALT was observed during this period. We thus suspected that antigenic stimulation by a lower level of viral growth in the liver, which remained below detectable levels in blood, might lead to the induction of the anti-NS3 antibody and the recurrent ALT increase. Subsequently, viremia became detectable at week 58 p.i. and $10^4$–$10^5$ copies/ml of the viral RNA persisted until week 108 p.i. Thereafter, an abrupt increase of the anti-core antibody was detected, concomitant with augmentation of the viral load of $10^{5.5}$ copies/ml on average and recurrent increases in the ALT level. Eventually, the individual was euthanized at week 229 p.i. because of poor prognosis since the ALT value drastically increased by 161-fold, which was accompanied by a dramatic decrease of platelet counts and a deteriorating general status. Histopathological analyses of the necropsy samples demonstrated that the liver developed diffuse piecemeal necrosis with infiltration of lymphocytes and

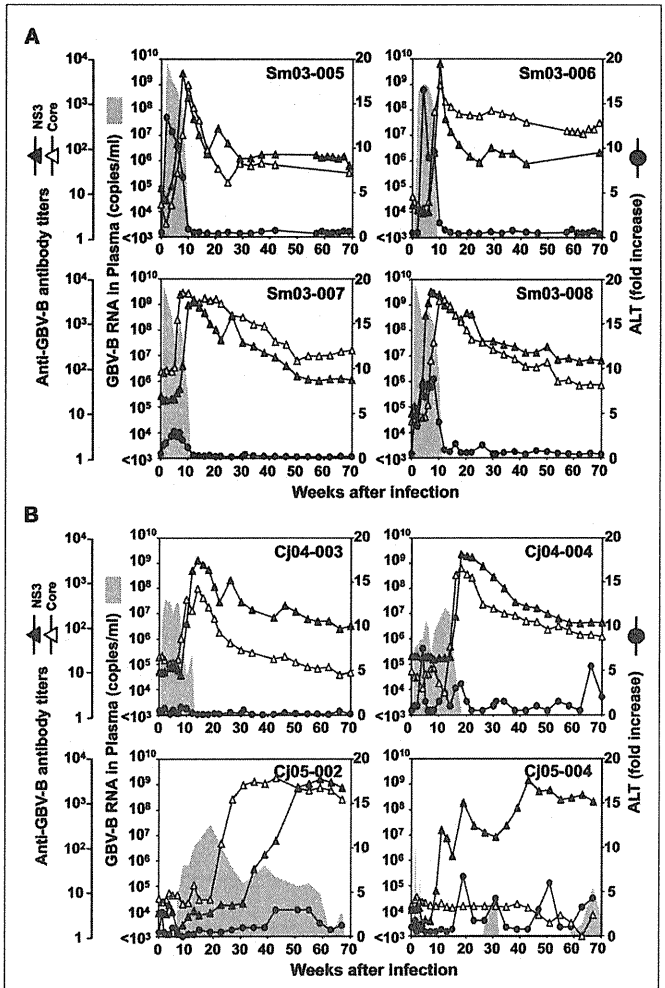


**FIGURE 1 | Infection profiles until week 70 p.i. of tamarins (A) and marmosets (B) inoculated intrahepatically with GBV-B infectious serum obtained from a tamarin.** Plasma samples periodically obtained from the monkeys were evaluated for the copy numbers of GBV-B genomic RNA (green shaded area), ALT levels (red circles), and the antibody titers against GBV-B core and NS3 (blue and yellow triangles, respectively).

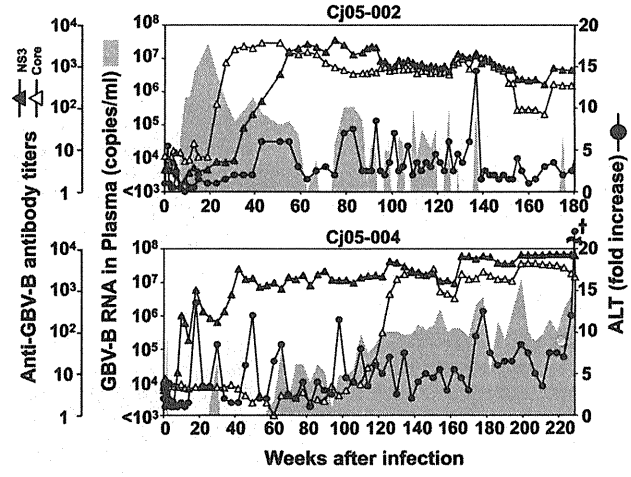


**FIGURE 2 | Profiles of the marmosets persistently infected with GBV-B.** Plasma samples periodically obtained from the marmosets were evaluated for the copy numbers of GBV-B genomic RNA (green shaded area), ALT levels (red circles), and the antibody titers against GBV-B core and NS3 (blue and yellow triangles, respectively). The cruciate mark in Cj05-004 indicates that the individual was euthanized due to a poor prognosis at week 229 p.i. At that time, the ALT value in plasma had increased by 161-fold.

formation of lymphoid follicles (**Figure 3A**, Appendix). The viral load in the liver was relatively high ($3.8 \times 10^4$ copies/mg tissue weight), which was similar to the viral load observed for tamarins acutely infected with GBV-B (Ishii et al., 2007). The high viral load in the liver was consistent with a large number of granular positive signals for the core protein, which was in similar manner with the core protein of HCV (Miyanari et al., 2007), as immunostained with an anti-GBV-B core monoclonal antibody (**Figure 3B**). Notably, Masson trichrome staining (**Figures 3C,D**) as well as Elastica van Gieson staining (Appendix) demonstrated that the liver also developed diffuse and abundant fibrosis. The disease of this marmoset was therefore diagnosed as a case of acute exacerbation of progressive chronic hepatitis by GBV-B infection.

## ANALYSIS OF MUTATIONS IN GBV-B GENOMES

Next, we determined the dominant sequence of the viral genomes at weeks 45, 104, and 135 p.i. in Cj05-002 and weeks 33, 88, 141, and 229 p.i. in Cj05-004. As seen in **Figure 4A**, it was found that there was no specific region in which extensive nucleotide mutations occurred throughout the study periods and that the nucleotide mutation rates were $1.9–2.9 \times 10^{-3}$ and $1.5–3.6 \times 10^{-3}$ changes per site per year in Cj05-002 and Cj05-004, respectively (**Table 1**). In terms of amino acid substitution, we observed the following: (i) several back or sequential mutations (G250V > A, S731L > S, E2346G > E in Cj05-002; V254A > V, I285V > I, L495S > L, T735A > T, F2135L > F > S in Cj05-004) in both marmosets; (ii) highly selective non-synonymous mutations that were remarkable in E1, but such mutations were rarely observed in core (**Figures 4** and **5**); and (iii) the non-synonymous mutation rates were $1.8–4.0 \times 10^{-3}$ and $2.1–4.6 \times 10^{-3}$ substitutions per site per year in Cj05-002 and Cj05-004, respectively (**Figures 4** and **5; Table 2**). (iv) The non-synonymous changes detected mainly in NS5A and NS5B in both animals were also observed in a number of previous reports (Simons et al., 1995; Bukh et al., 1999; Sbardellati et al., 2001; Martin et al., 2003; Nam et al., 2004; Kyuregyan et al., 2005; Weatherford et al., 2009; Takikawa et al., 2010). It may be reasonable to consider that the molecular clone we employed (Bukh et al., 1999) was derived from a minor clone of mixed populations and emergence of a new mutations easily occurred as a mechanism of GBV-B adaptation to a new host, while it is also possible that "consensus" non-synonymous changes were due to either a result of a selection of the pre-existent minor variants. Taken together, these results suggest that efficient

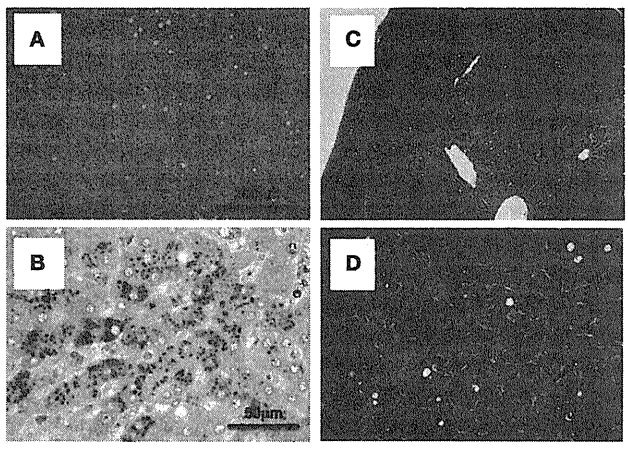


**FIGURE 3 | Histopathological and immunohistochemical analyses of the liver from Cj05-004 at week 229 p.i. HE staining (A), immunohistochemical staining for the core protein of GBV-B (B), and Masson's trichrome staining (C,D) are shown.**

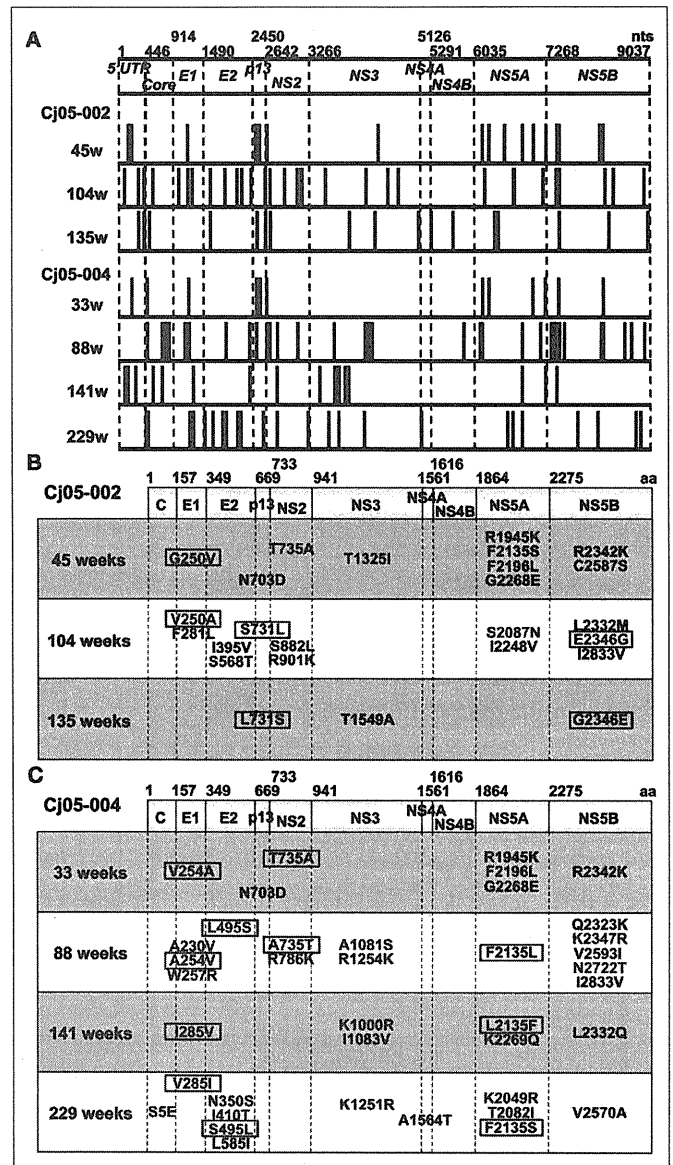


**FIGURE 4 | Mutations in the viral genome sequences amplified from plasma of the marmosets persistently infected with GBV-B. (A)** Positions of the nucleotide mutations in the viral genome sequences at multiple time points (at weeks 45, 104, and 135 in Cj05-002 and weeks 33, 88, 141, and 229 in Cj05-004) are illustrated as bars. **(B,C)** Positions of the non-synonymous mutations in the viral genome sequences at multiple time points are shown. **(B)** Cj05-002; **(C)** Cj05-004. Positions of the mutations that had been identified in previous reports are indicated as black, while those unidentified previously are shown as blue. Red squares illustrate back or sequential mutations.

**Table 1 | Summary of the nucleotide substitutions in GBV-B genome sequences amplified from plasma of the marmosets persistently infected with GBV-B.**

| Genomic region | nt position | No. (%) of nt differences | | | | | | |
|---|---|---|---|---|---|---|---|---|
| | | Cj05-002 | | | Cj05-004 | | | |
| | | 45 weeks | 104 weeks | 135 weeks | 33 weeks | 88 weeks | 141 weeks | 229 weeks |
| 5′UTR | 1–445 | 2 (0.45) | 3 (0.67) | 2 (0.45) | 1 (0.22) | 0 (0) | 3 (0.67) | 0 (0) |
| Core | 446–913 | 0 (0) | 1 (0.21) | 1 (0.21) | 1 (0.21) | 4 (0.85) | 2 (0.43) | 3 (0.64) |
| E1 | 914–1489 | 1 (0.17) | 3 (0.52) | 0 (0) | 1 (0.17) | 3 (0.52) | 1 (0.17) | 2 (0.35) |
| E2 | 1490–2449 | 0 (0) | 5 (0.52) | 1 (0.10) | 0 (0) | 2 (0.21) | 1 (0.10) | 6 (0.63) |
| p13 | 2450–2641 | 2 (1.04) | 1 (0.52) | 2 (1.04) | 2 (1.04) | 1 (0.52) | 0 (0) | 1 (0.52) |
| NS2 | 2642–3265 | 1 (0.16) | 5 (0.80) | 1 (0.16) | 1 (0.16) | 4 (0.64) | 1 (0.16) | 2 (0.32) |
| NS3 | 3266–5125 | 1 (0.05) | 4 (0.22) | 3 (0.16) | 0 (0) | 5 (0.27) | 6 (0.32) | 3 (0.16) |
| NS4A | 5126–5290 | 0 (0) | 0 (0) | 0 (0) | 0 (0) | 0 (0) | 0 (0) | 1 (0.61) |
| NS4B | 5291–6034 | 0 (0) | 0 (0) | 2 (0.27) | 0 (0) | 1 (0.13) | 0 (0) | 0 (0) |
| NS5A | 6035–7267 | 6 (0.49) | 4 (0.32) | 2 (0.16) | 4 (0.32) | 4 (0.32) | 2 (0.16) | 3 (0.24) |
| NS5B | 7268–9037 | 4 (0.23) | 5 (0.28) | 3 (0.17) | 2 (0.11) | 10 (0.56) | 1 (0.06) | 4 (0.23) |
| Total | 9037 | 17 (0.19) | 31 (0.34) | 17 (0.19) | 12 (0.13) | 34 (0.38) | 17 (0.19) | 25 (0.28) |
| Mutation rate/year | | $2.2 \times 10^{-3}$ | $3.0 \times 10^{-3}$ | $3.2 \times 10^{-3}$ | $2.1 \times 10^{-3}$ | $3.6 \times 10^{-3}$ | $1.8 \times 10^{-3}$ | $1.6 \times 10^{-3}$ |

**Table 2 | Summary of the amino acid substitutions in GBV-B genome sequences amplified from plasma of the marmosets persistently infected with GBV-B.**

| Amino acid region | aa position | No. (%) of aa differences | | | | | | |
|---|---|---|---|---|---|---|---|---|
| | | Cj05-002 | | | Cj05-004 | | | |
| | | 45 weeks | 104 weeks | 135 weeks | 33 weeks | 88 weeks | 141 weeks | 229 weeks |
| Core | 1–156 | 0 (0) | 0 (0) | 0 (0) | 0 (0) | 0 (0) | 0 (0) | 1 (0.64) |
| E1 | 157–348 | 1 (0.52) | 2 (1.04) | 0 (0) | 1 (0.52) | 3 (1.56) | 1 (0.52) | 1 (0.52) |
| E2 | 349–613 | 0 (0) | 2 (0.63) | 0 (0) | 0 (0) | 1 (0.31) | 0 (0) | 4 (1.25) |
| P13 | 669–732 | 1 (1.56) | 1 (1.56) | 1 (1.56) | 1 (1.56) | 0 (0) | 0 (0) | 0 (0) |
| NS2 | 733–940 | 1 (0.48) | 2 (0.96) | 0 (0) | 1 (0.48) | 2 (0.96) | 0 (0) | 0 (0) |
| NS3 | 941–1560 | 1 (0.16) | 0 (0) | 1 (0.16) | 0 (0) | 2 (0.32) | 2 (0.32) | 1 (0.16) |
| NS4A | 1561–1615 | 0 (0) | 0 (0) | 0 (0) | 0 (0) | 0 (0) | 0 (0) | 1 (1.82) |
| NS4B | 1616–1863 | 0 (0) | 0 (0) | 0 (0) | 0 (0) | 0 (0) | 0 (0) | 0 (0) |
| NS5A | 1864–2274 | 4 (0.97) | 2 (0.49) | 0 (0) | 3 (0.73) | 1 (0.24) | 2 (0.49) | 3 (0.73) |
| NS5B | 2275–2864 | 2 (0.34) | 3 (0.51) | 1 (0.17) | 1 (0.17) | 5 (0.85) | 1 (0.17) | 1 (0.17) |
| Total | 2864 | 10 (0.38) | 12 (0.42) | 3 (0.10) | 7 (0.24) | 14 (0.49) | 6 (0.21) | 12 (0.42) |
| Mutation rate/year | | $4.0 \times 10^{-3}$ | $3.7 \times 10^{-3}$ | $1.8 \times 10^{-3}$ | $3.9 \times 10^{-3}$ | $4.6 \times 10^{-3}$ | $2.1 \times 10^{-3}$ | $2.5 \times 10^{-3}$ |

and selective evasion from immune pressure in the two marmosets resulted in long-term persistent GBV-B infection accompanied by subsequent chronic hepatitis.

## DISCUSSION

In this study, we show for the first time that GBV-B is capable of eliciting a chronic and progressive hepatitis C-like disease in marmosets. Evidence for this condition is demonstrated by long-term persistent GBV-B infection, recurrent ALT increase, and fibrosis. Moreover, one of the chronically infected marmosets developed acute exacerbation of chronic hepatitis as indicated by diffuse piecemeal liver necrosis and an ALT flare, which is seen in patients with viral hepatitis (Perrillo, 1997). While the usefulness of the monkey model as a surrogate model for HCV infection has been under debate due to the virtual inability of GBV-B to cause chronic hepatitis C-like disease in tamarins, the present data demonstrate that the ability of GBV-B to induce the chronic disease is likely to be inherent depending on the differences between species and individuals.

It has been reported that tamarins generally permit extensive replication of GBV-B in the subacute phase of infection and develop acute hepatitis as shown by significant increases of serum enzymes such as ALT and isocitrate dehydrogenase. The viral load in marmosets seems to be lower than in tamarins (Lanford et al.,